MDPI

Review

New Advances in Materials, Applications, and Design Optimization of Thermocline Heat Storage: Comprehensive Review

Yunshen Zhang, Yun Guo *, Jiaao Zhu, Weijian Yuan and Feng Zhao

School of Mechanical and Automotive Engineering, Shanghai University of Engineering Science, Shanghai 201620, China; m310121501@sues.edu.cn (Y.Z.); m310122512@sues.edu.cn (J.Z.); m310121508@sues.edu.cn (W.Y.); m310121515@sues.edu.cn (F.Z.)
* Correspondence: 01050226@sues.edu.cn

Abstract: To achieve sustainable development goals and meet the demand for clean and efficient energy utilization, it is imperative to advance the penetration of renewable energy in various sectors. Energy storage systems can mitigate the intermittent issues of renewable energy and enhance the efficiency and economic viability of existing energy facilities. Among various energy storage technologies, thermocline heat storage (THS) has garnered widespread attention from researchers due to its stability and economic advantages. Currently, there are only a few review articles focusing on THS, and there is a gap in the literature regarding the optimization design of THS systems. Therefore, this paper provides a comprehensive review of the recent research progress in THS, elucidating its principles, thermal storage materials, applications, and optimization designs. The novelty of this work lies in the detailed classification and analysis of various optimization designs for THS, including tank shape, aspect ratio, inlet/outlet configuration, thermal energy storage materials arrangement, operating strategies, and numerical model optimization approaches. The limitations of existing research are also identified, and future perspectives are proposed, aiming to provide recommendations for THS research and contribute to the development and promotion of THS technology.

1. Introduction

With the increase in the world population and the improvement of living standards, there is a continuous rise in energy demand [1]. However, the excessive use of non-renewable energy sources has led to increasingly severe environmental issues, such as extreme weather events, global warming, and air pollution [2]. The utilization of renewable and clean energy sources, improvement of the efficiency of existing energy consumption systems, and reduction in energy losses are key approaches to addressing energy challenges.

Energy storage technologies offer various advantages to energy systems, including increasing the penetration of renewable energy, enhancing energy efficiency, and improving economic viability [3]. Thermal energy storage (TES) technology stands out as a crucial energy storage method capable of reducing disparities between energy demand and supply. It finds widespread applications in areas such as harnessing new energy sources, waste heat recovery, and desalination [4].

According to the TES mechanism, TES technology can be divided into three categories: sensible heat storage, latent heat storage, and thermo-chemical heat storage. Thermocline heat storage (THS), a method that can integrate with the above three TES technologies, stores both cold and hot heat transfer fluids (HTFs) and TES media in the same tank. Due to the effects of density difference and buoyancy, the cold and hot fluids automatically stratify within the tank, forming a temperature gradient zone known as the thermocline

zone. In comparison to traditional two-tank TES systems, THS systems have a simpler structure, occupy less space, and can save 15–45% in costs [5,6]. Cascetta's techno-economic comparison indicates that the leveling storage cost of a single-tank system is approximately 48% lower than that of a two-tank TES system [7]. Consequently, THS technology has become a recent research focus. Enhancing the efficiency, reducing costs, and promoting the widespread application of THS systems are the current primary research directions.

An analysis of the number of articles published from 2010 to 2023 indicates an overall upward trend in the volume of research related to THS, as depicted in Figure 1. However, only a handful of reviews have specifically focused on THS. Despite numerous studies dedicated to the optimization of THS systems, there has been an absence of a comprehensive summary and review of the various optimization methodologies.
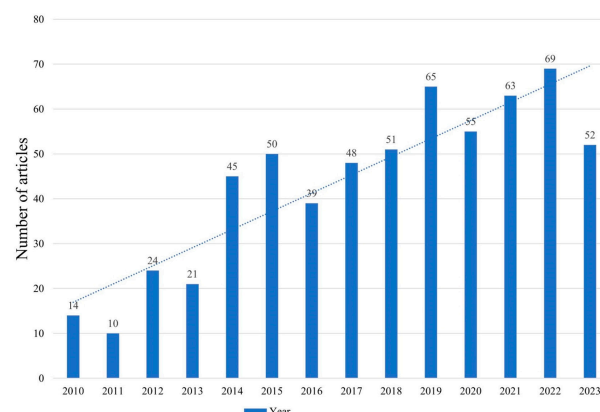

Figure 1. Number of articles on THS from 2010 to 2023.

This paper presents a synthesis of the recent advancements in THS research, providing a thorough exposition of the principles, thermal energy storage materials (TESMs), applications, and optimization approaches associated with THS. In terms of TESMs, this review summarizes the thermal properties of the majority of liquid and solid materials utilized in THS and introduces several novel materials, providing insights into material selection in TES system design and facilitating the promotion of new materials. The discussion of THS applications reveals its compatibility with various systems and the economic or environmental benefits it can provide.

The focal point of this paper is the classification, analysis, and summarization of THS optimization methods, offering comprehensive information for the improvement of existing THS systems and the design of new ones. This contributes to enhancing the efficiency, economic viability, and compatibility of THS systems, thereby facilitating the broader application and promotion of this technology and contributing to energy conservation. Finally, by reviewing the most recent studies, we have identified the shortcomings in current research and propose several suggestions and prospects for future work.

2. Thermocline Heat Storage Principles

2.1. Basic Principles

The basic principle of THS is to utilize the density difference between cold and hot fluids to form natural stratification. When the hot fluid is injected from the top of the storage tank, due to its lower density, it will stay at the upper part of the tank, whereas since the cold fluid is drawn from the bottom of the tank, due to its higher density, it settles at the lower part of the tank. Inside the storage tank, a distinct temperature gradient is formed, known as the "thermocline". THS stores heat through the TESM inside the tank, which can be divided into sensible TESMs and latent TESMs (as known as phase change materials, PCMs). The sensible TESM stores and releases heat through the change

in material temperature, and its specific heat capacity determines the heat storage capacity of the sensible TESM. The calculation formula of sensible TES can be expressed as follows:

$$Q_s = mc\Delta T \tag{1}$$

where Q_s represents the amount of sensible heat stored or released, m is the mass of the material, c is the specific heat capacity, and ΔT is the change in temperature.

Latent TES, which utilizes PCMs, operates on the principle of absorbing or releasing latent heat during the phase transition process. Throughout this process, the temperature of the PCM remains constant, yet it is capable of absorbing or releasing a substantial amount of thermal energy. The calculation formula of latent TES (Q_L) can be expressed as follows:

$$Q_L = \int_{T_i}^{T_m} mcdT + ma_m\Delta h_m + \int_{T_m}^{T_e} mcdT \tag{2}$$

where T_i and T_e are the initial temperature and the end temperature of the heat storage process, respectively; a_m is the melting fraction, Δh_m is the latent heat per unit mass, and T_m is the melting point of the medium.

The heat stored in a THS system is the sum of the heat stored in the sensible TESMs and PCMs inside the tank, expressed as follows:

$$Q_{THS} = Q_s + Q_L \tag{3}$$

2.2. Classification of Thermocline Heat Storage

Based on the different TESMs inside the tank, THS systems can be divided into single-medium thermocline heat storage (SMTHS) tanks and dual-medium thermocline heat storage (DMTHS) tanks. In SMTHS tanks, only the HTF itself serves as the thermal storage medium, while in DMTHS tanks, both the solid TESM and HTF serve as the thermal storage medium simultaneously. SMTHS tanks are characterized by their simple structure, convenient construction, easy maintenance, and high thermal efficiency but relatively low energy storage capacity. The solid TESM in DMTHS tanks can increase the heat storage capacity, but it may introduce issues such as thermal ratcheting, particle deposition leading to maintenance problems, material compatibility issues, and thermal losses due to heat exchange. In some high-temperature applications, a solid TESM has replaced some expensive liquid TESMs, thereby reducing costs. DMTHS tanks can be further subdivided into packed bed THS tanks and structured THS tanks. Packed beds can be classified based on the arrangement of solid TESM particles into disordered beds, ordered beds, cascaded beds, segmented beds, and layered beds, which will be detailed in Section 5.

Based on whether heat exchangers or heat exchange coils are used for heat exchange, THS systems can be categorized as direct systems (also known as open systems) and indirect systems (closed systems). The THS system types introduced in this article are shown in Figure 2.
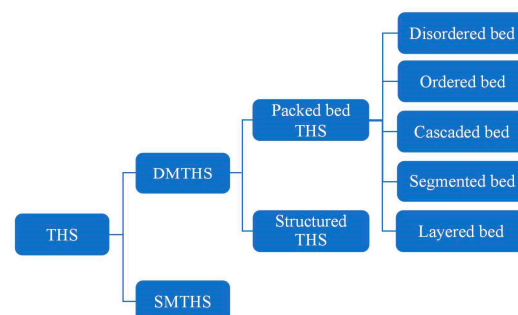

Figure 2. Classification of THS systems.

2.3. Thermocline Heat Storage Process

THS tanks operate in three modes: charging (energy storage), discharging (energy release), and standby mode. During charging, a high-temperature HTF is typically injected from the top inlet of the tank, while a cold HTF is expelled from the bottom port. Due to the density difference and buoyancy, the cold and hot fluids separate into an upper hot temperature zone and a lower cold temperature zone. Heat diffusion between the cold and hot fluids creates a thermal stratification zone with a temperature gradient known as the thermocline zone. As the charging time increases, the thermocline zone moves downward, expanding continuously until the outlet temperature reaches the cut-off temperature, stopping the charging process. During discharging, the low-temperature HTF enters from the bottom of the tank, and the thermocline zone moves upward. During the charging and discharging process, the heat imbalance and uneven flow in the tank will cause the hot and cold fluids to form convection or vortex, reducing thermal stratification, resulting in a reduction in the energy storage capacity and overall efficiency of the storage tank. The schematic diagram of the thermocline is shown in Figure 3.
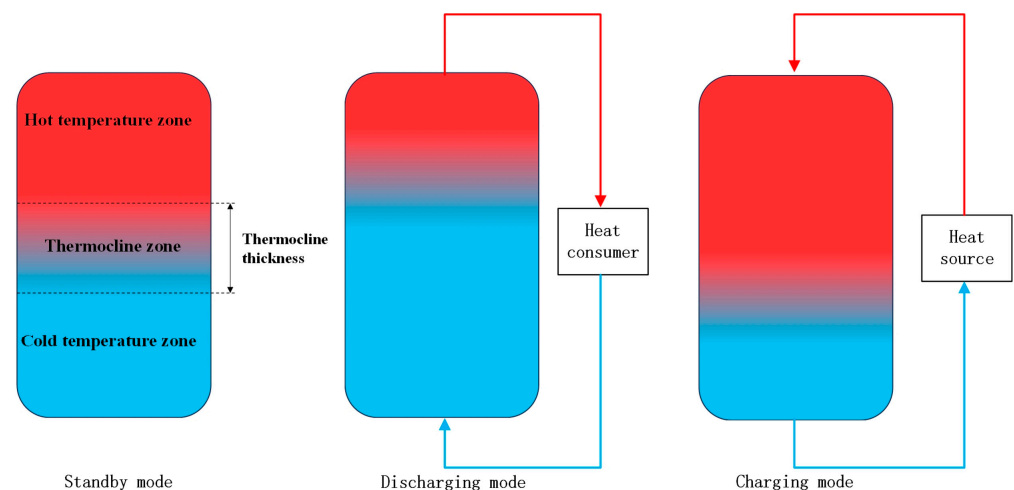

Figure 3. A schematic diagram of the thermocline.

In the literature, different methods define the thermocline zone, including the percentage of the maximum temperature difference in the fluid [8], absolute value of the temperature difference [9], or based on the magnitude of the temperature gradient. The thickness and stability of the thermocline significantly impact the performance of THS tanks, with thinner thermoclines leading to better tank performance.

During charging, the injection of thermal jets causes entrainment phenomena [10], resulting in convective heat transfer and fluid dynamic perturbations [11], leading to thermocline decay. Obtaining piston flow and the flattened thermocline shape during charging and discharging is essential for ensuring proper thermal stratification. Due to the lack of solid filler buffering, thermoclines in SMTHS tanks are more affected by thermal jets. Precise analytical solutions for convective heat transfer caused by buoyancy jets in SMT tanks have been established [12]. Yi and Nakayama developed a set of volume-averaged control equations to study transient convection and heat conduction in a packed bed THS tank. They determined three crucial dimensionless parameters: the solid-to-liquid heat capacity ratio, the gap Stanton number, and the Peclet number based on effective total thermal conductivity and derived explicit expressions for the effective discharge efficiency [13].

The expansion rate of the thermocline region varies with the filling material. The interface formed between two different filling materials affects the development of the thermocline. When the thermocline region moves from a slower-expanding material to a faster-expanding one, the thermocline thickness increases, known as the expansion effect. Conversely, when it moves from a faster-expanding material to a slower one, it decreases, termed the contraction effect. This interface effect can be utilized to control the development

of the thermocline. Li et al. utilized a transient two-dimensional axisymmetric model to analyze the cycling performance of traditional single-layer packed bed THS tanks and new multi-layer packed bed THS tanks [14]. They optimized the new multi-layer packed bed THS tank using the interface effect. After optimization with three types of filling materials (quartzite, cast iron, and high-temperature concrete), the tank's effective energy was increased by 10.5% compared to a tank filled solely with quartzite, with a slight decrease of 2.1% in thermal efficiency. Xie et al. found that heat loss has a significant impact on thermocline expansion (>20%), and good insulation can increase charging efficiency by 5–7% and the capacity ratio by 3–5% [15].

When the tank is in standby mode, the water body remains in a static state, allowing the thermocline to persist for an extended period. However, due to the influence of axial temperature gradients and radial temperature gradients caused by wall heat losses, the thickness of the thermocline continually increases, and the expansion rate gradually decreases. The higher the initial position of the thermocline, the faster the temperature decrease in the high-temperature fluid [16]. Therefore, it is advisable to avoid long periods of standby mode for the tank and apply necessary thermal insulation to the tank.

2.4. Thermal Ratchet Phenomenon

The phenomenon of thermal ratcheting may occur in DMTHS tanks during consecutive cycles of heating and cooling, posing a concern in engineering applications that could compromise the safety and structural integrity of the tank [17]. During the charging process, if the thermal expansion of the tank wall exceeds that of the filling material, a radial gap may form, causing the settling of the filling material due to gravitational forces. In the discharging process, the settled particles cannot return to their original positions, occupying space and preventing the tank from fully contracting, leading to thermal stress and potential plastic deformation. The continuous deformation of the tank wall during the cycling process can result in structural damage.

Significant research has been conducted on the thermal ratcheting phenomenon in THS tanks. Elfeky et al. developed a two-phase numerical method to investigate the impact of the melting temperature of phase change material (PCM) layers on the thermo-mechanical performance of cascading thermal stratification storage tanks [18]. The study considered the thermal interactions between PCM capsules, insulation layers, the fluid, the environment, and the shell. Additionally, the research assessed the risk of ratcheting failure. González et al. proposed an original numerical model that was dynamically solved in the NEST platform and coupled all important components of the CSP plant energy storage system, allowing for the analysis of the thermo-mechanical parameters of the packed bed THS tank during plant operation [19]. They suggested representing tank wall stress using hoop stress, as under equivalent stress, the effects of radial stress, structural self-weight, and high-temperature gradient bending can be negligible.

Flueckiger et al. developed a modeling approach that simulates fluid flow and heat transfer within the tank using a two-temperature model [17]. Finite element analysis was employed to predict the thermo-mechanical stress associated with thermal ratcheting. The study investigated the possibility of thermal ratcheting-induced damage to the composite wall structure of DMTHS tank shells, with results suggesting that enhancing the insulation performance inside the tank can reduce the likelihood of thermal ratcheting. Wang et al. established a numerical model of a multi-layer wall structure THS tank and conducted a comprehensive parameter study on the comprehensive thermal and mechanical performances of the tank [20]. Studies have shown that the maximum mechanical stress on the tank wall can be reduced by increasing the inlet HTF temperature and velocity or reducing the diameter, thermal conductivity, and specific heat of solid filler particles.

The application of a structured packed bed [21] and orderly arrangement of solid fillers can also avoid the thermal ratchet phenomenon.

2.5. Dimensionless Numbers and Performance Indicators

2.5.1. Dimensionless Numbers

This section introduces commonly used dimensionless numbers related to THS, which can describe and characterize THS systems.

- Stratification number

The stratification number is defined as the ratio of the mean of the temperature gradients at any time interval to the maximum mean temperature gradient for the charging–discharging process. The stratification number is expressed as

$$Str = \frac{\partial T/\partial y}{(\partial T/\partial y)_{\max}} \tag{4}$$

- Dimensionless temperature

$$T^* = \frac{T - T_c}{T_h - T_c} \tag{5}$$

- Reynolds number

The Reynolds number represents a ratio of the inertial to the viscous forces.

The Reynolds number of inlet/outlet ports can be expressed as follows:

$$Re = \frac{\rho_f v_f d}{\mu_f} \tag{6}$$

where ρ_f is the density of the fluid, v_f is the superficial velocity of the fluid, d is the diameter of inlet/outlet port, and μ_f is the viscosity of the fluid.

The Reynolds number of a storage tank can be expressed as follows:

$$Re_{tank} = \frac{\rho_f \overline{v}_{tank} W}{\mu_f} \tag{7}$$

where W is the side length of the storage tank; $\overline{v}_{tank}$ is the average velocity of the fluid inside the tank.

The Reynolds number of TES material particles can be expressed as follows [22]:

$$Re_p = \frac{\rho_f v_f d_p}{\mu_f(1 - \varepsilon)} \tag{8}$$

where d_p is the diameter of the particle, and ε is the void fraction of the packed bed.

- Richardson number

It is a measure of the ratio of the buoyancy to the mixing force and provides qualitative estimates for thermal stratification in storage tanks. For low flow rates, the Richardson number is bigger, representing better stratification within the tank [23]. At low flow rates, the Richardson number can qualitatively represent stratification in storage tanks. Under charging conditions with highly variable fluid flow rates, the Richardson number should not be used to characterize thermal stratification [22].

$$Ri = \frac{g\beta H \cdot (T_{top} - T_{bottom})}{\overline{v}_{tank}^2} \tag{9}$$

where g is the gravitational acceleration, β is the thermal expansion coefficient, H is the height of the storage tank, T_{top} is the temperature at the top of the storage tank, and T_{bottom} is the temperature at the bottom of the storage tank.

- Froude number

Froude number (*Fr*) is defined as the ratio of inertial force and the buoyancy force.

$$Fr = \frac{\overline{v}_{in}}{\sqrt{d_p g(\rho_c - \rho_h)/\rho_c}} \tag{10}$$

where ρ_c is the density of cold fluid, ρ_h is the density of hot fluid, and $\overline{v}_{in}$ is the average velocity of the inlet port.

- Peclet number

The Peclet number provides the relationship between bulk heat transfer and conductive heat transfer. It is usually used together with the Richardson number to define stratification in storage tanks [23]. The Pe number cannot be evaluated separately for thermal stratification, as it increases with increasing flow rate.

$$Pe = \frac{vH}{\alpha} \tag{11}$$

where

$$v = \frac{Q}{\pi \cdot r_{tank}^2} \tag{12}$$

where Q is the flow rate of the HTF, and α is the thermal diffusivity of the HTF; r_{tank} is the radius of the storage tank.

- Stanton number

The Stanton number contains the heat transfer information and can be thought of as a ratio of temperature differences and areas. The authors of Ref. [24] proposed that the higher the St value, the better the effective heat transfer coefficient. The Stanton number can be expressed as follows:

$$St = \frac{h}{\rho_f C_{p_f} u} \tag{13}$$

where h is the convective heat transfer coefficient; u is the fluid velocity.

- MIX number

The MIX number considers different temperature distributions inside the tank and divides the tank into several volumes at different temperatures. The MIX number can be used to characterize the stratification inside a water tank, but it is highly sensitive to small changes in operating temperature and temperature curves, and it is necessary to measure the water temperature inside the tank, making it difficult to use [23].

The range of MIX numbers is from 0 to 1, where MIX = 0 represents a fully layered tank, and MIX = 1 represents a perfectly mixed tank. The MIX number can be expressed as follows:

$$MIX = \frac{M_{str} - M_{exp}}{M_{str} - M_{fully-mixed}} \tag{14}$$

where M_{exp} is the momentum of energy derived from experimental data, M_{str} is the momentum of energy for a perfectly stratified storage, and $M_{fully-mixed}$ is the momentum of energy of a perfectly mixed storage. Both M_{str} and $M_{fully-mixed}$ are calculated for TES, storing the same amount of energy as derived from the experimental data.

Joseph Rendall et al. reviewed ten dimensionless numbers (Archimedes, Biot, Froude, Grassof, Peclet, Rayleigh, Reynolds, Richardson, Atwood, Stratification) used for modeling THS tanks, with a focus on the Richardson number and Reynolds number [25].

2.5.2. Performance Indicators

A key performance parameter is storage efficiency, defined as the ratio between the increase in stored internal energy and the net thermal energy flowing into the storage tank [26].

$$\eta_s = \frac{E_{store}}{E_{net}} = \frac{E_{store}}{\int_0^t \dot{m} C_p (T_{in} - T_{out}) dt} \tag{15}$$

In some of the literature [27], energy storage efficiency is defined as follows:

$$\eta = \frac{E_{discharged}}{E_{charged} + E_{pumping}} \tag{16}$$

And

$$E_{charged/discharged} = \int_0^t \dot{m} C_p (T_{in} - T_{out}) dt \tag{17}$$

The capacity ratio (σ) represents the ratio of the actual stored thermal energy to the maximum storage capacity of the THS tank.

$$\sigma = \frac{E_{store}}{E_{store}^{max}} = \frac{E_{store}}{V_{tank} \left(C_{p_{in}} T_{in} \rho_{in} - C_{p_c} T_c \rho_c \right)} \tag{18}$$

where the subscript *in* represents the state at the inlet of the tank, and *c* represents the initial state.

The charging efficiency based on the first law of thermodynamics is as follows [28]:

$$\eta_{ch}(t) = \frac{T_{avg}(t) - T_{ini}}{T_{inlet} - T_{ini}} \tag{19}$$

where $T_{avg}(t)$ is the average temperature of the tank over time, T_{ini} is the initial average temperature of the tank, and T_{inlet} is the inlet temperature of the tank. When the inlet temperature of the storage tank also changes over time, Equation (19) can be written as follows:

$$\eta_{ch}(t) = \frac{T_{avg}(t) - T_{ini}}{T_{inlet}(t) - T_{ini}} \tag{20}$$

The exergy charging efficiency based on the second law of thermodynamics can be expressed as follows:

$$\eta_{ex} = 1 - \frac{T_0}{H(T_{del} - T_{mean})} \int_0^H \ln \left(\frac{T_{del}}{T_{(y)}} \right) dy \tag{21}$$

where T_0 is the dead state or reference temperature, H is the height of the tank, T_{del} is the exergy delivery temperature, T_{mean} is the mean temperature of the storage, and y is the vertical coordinate of the tank. In the experiment, Equation (21) was discretized, and T_{mean} is equal to T_{avg}, and T_{del} is equal to T_{inlet}, giving the following:

$$\eta_{ex} = 1 - \frac{T_0}{H(T_{inlet} - T_{avg})} \sum_{i=1}^{N} \ln \left(\frac{T_{inlet}}{T_i} \right) \Delta h \tag{22}$$

The energy efficiency calculated based on the stored fluid flow rate is as follows [29]:

$$\eta_{en} = \frac{\int_{t_d} \dot{m} \cdot \left(h_m \left(T_f^{out,d} \right) - h_m \left(T_f^{in,d} \right) \right) dt}{\int_{t_{ch}} \dot{m} \cdot \left(h_m \left(T_f^{in,ch} \right) - h_m \left(T_f^{out,ch} \right) \right) dt} \tag{23}$$

where h_m is the specific enthalpy; the fluid temperatures at the inlet and outlet of the tank are $T_f^{in,d}$ and $T_f^{out,d}$, while the superscripts *ch* and *d* correspond to the charging and

discharging processes, respectively. From a physical perspective, energy efficiency is an indicator of the quality of the tank's insulation. In the adiabatic case, it is equal to 1 in stationary periodic operation. And exergy efficiency can be expressed as follows:

$$\eta_{ex} = \frac{\int_{t_d} \dot{m} \cdot \left(h_m \left(T_f^{out,d} \right) - h_m \left(T_f^{in,d} \right) \right) dt \cdot \left(1 - \frac{T_\infty}{\widetilde{T}_d} \right)}{\int_{t_{ch}} \dot{m} \cdot \left(h_m \left(T_f^{in,ch} \right) - h_m \left(T_f^{out,ch} \right) \right) dt \cdot \left(1 - \frac{T_\infty}{\widetilde{T}_{ch}} \right)} \tag{24}$$

where T_∞ is the average ambient temperature; $\widetilde{T}$ is the entropic mean temperature of the transformation.

$$\widetilde{T}_{ch} = \frac{\int_{t_{ch}} \dot{m} \cdot \left(h_m \left(T_f^{in,ch} \right) - h_m \left(T_f^{out,ch} \right) \right) dt}{\int_{t_{ch}} \dot{m} \cdot \left(s_m \left(T_f^{in,ch} \right) - s_m \left(T_f^{out,ch} \right) \right) dt} \tag{25}$$

$$\widetilde{T}_d = \frac{\int_{t_d} \dot{m} \cdot \left(h_m \left(T_f^{out,d} \right) - h_m \left(T_f^{in,d} \right) \right) dt}{\int_{t_d} \dot{m} \cdot \left(s_m \left(T_f^{out,d} \right) - s_m \left(T_f^{in,d} \right) \right) dt} \tag{26}$$

The ratio of energy efficiency to exergy efficiency is defined as the storage quality factor Ψ_s, whose value only depends on the average entropy temperature and can be used to quantify the exergy loss during energy storage.

$$\Psi_s = \frac{\eta_{ex}}{\eta_{en}} = \frac{\left(1 - \frac{T_\infty}{\widetilde{T}_d} \right)}{\left(1 - \frac{T_\infty}{\widetilde{T}_{ch}} \right)} \tag{27}$$

The first law thermodynamic round-trip efficiency (*RTE*) of the storage process can be defined here as the ratio of the heat recovered during discharge to the heat stored during charge and is given by the following [30]:

$$RTE = \frac{Q_d}{Q_c} = \frac{\int_{t_c}^{t_d} \left[\dot{m} c_p \left(T_{top} - T_{bot} \right) \right] dt}{\int_0^{t_c} \left[\dot{m} c_p \left(T_{top} - T_{bot} \right) \right] dt} \tag{28}$$

The second law round-trip exergy efficiency (RTE_2). The fractional exergy or available work efficiency is defined as the ratio of the net exergy stored during charge to net exergy recovered during discharge and is given by the following [30]:

$$RTE_2 = \frac{B_d}{B_c} = \frac{\int_{t_c}^{t_d} \left[\dot{m}_g c_p \left(T_{bot} - T_{top} - T_{amb} ln(\frac{T_{bot}}{T_{top}}) \right) \right] dt}{\int_0^{t_c} \left[\dot{m}_g c_p \left(T_{top} - T_{bot} - T_{amb} ln(\frac{T_{top}}{T_{bot}}) \right) \right] dt} \tag{29}$$

2.5.3. Economic Indicators

The economic evaluation of the THS system is mainly carried out through two indicators: the levelized cost of storage (LCOS) [31] and the levelized cost of heat (LCOH) [32].

$$LCOS = \frac{CAPEX + \psi}{B} \tag{30}$$

where *CAPEX* is the cost of the THS system, ψ represents the total value of the exergy that will be stored in the THS throughout its lifespan, and *B* is the total exergy output of the THS throughout its lifespan.

The cost of a THS system comprises the combined costs of the TES system and associated equipment (such as water pumps). The TES system costs include the expenses

related to heat storage materials, tank construction, installation, insulation, and other associated components.

$$LCOH = \frac{f \cdot C + O}{E} \tag{31}$$

where f is the annuity factor, C is the capital cost, O is the operational cost, and E is the yearly energy yield.

And

$$f = \frac{d(1+d)^n}{(1+d)^n - 1} \tag{32}$$

with the discount rate d and the lifetime in years n.

2.5.4. Environmental Indicators

The environmental impacts of the THS system can be determined through Life Cycle Assessment (LCA), which is a standardized method [33]. For THS systems, four environmental indicators are considered:

- Cumulative Energy Demand (CED), measured in *MJ*, associated with the energy impact category.
- Global Warming Potential (GWP), measured in $kgCO_2$, associated with the climate change impact category.
- The Abiotic Depletion Potential (ADP) of minerals, fossil, and renewable resources, measured in $kgSb$, associated with the resource depletion impact category.
- Particulate Matter (PM), measured in kgPM2.5, associated with the human health impact category.

3. Thermal Energy Storage Materials for Thermocline Heat Storage

For various types and structures of THS systems, it is crucial to choose appropriate TESMs that meet thermal, physical, chemical, economic, and environmental requirements. The indicators to consider when selecting TESMs are as follows:

- Thermal indicators: specific heat capacity, melting point, thermal conductivity, thermal capacity heat transfer coefficient, and long-term thermal stability.
- Physics indicators: high physical stability and low expansion rate.
- Chemical indicators: high chemical stability, non-degradation, non-corrosiveness, non-toxicity, non-flammability, and non-explosiveness.
- Economic and environmental indicators: easy availability, cost-effectiveness, and environmental friendliness.

THSMs can be categorized based on their physical states into gas, liquid, and solid, with their thermal storage capacities increasing accordingly. Gaseous and liquid materials serve dual roles as HTFs and energy storage media in THS systems.

Air is the most common gaseous TESM, known for its stable chemical properties, wide operating temperature range, and cost-effectiveness. It is primarily used in applications such as solar thermal power plants [32,34], air heaters [35], and dryers [36]. Other inert gases, such as argon [30,37], are also used for THS.

Common liquid materials include water, thermal oil, and molten salt. Table 1 shows the thermal parameters of various liquid TESMs. The thermal properties of some liquid TESMs are sensitive to temperature changes, and their thermal properties can be expressed as a function of temperature, as shown in Table 2. In recent years, some researchers have studied the feasibility of using vegetable oil [38] and liquid metal [39] as TESMs. Water is inexpensive and non-toxic but has a narrow working range and is commonly used in household applications. Thermal oil and molten salt are mature commercial TESMs, and the use of molten salt requires attention to the freezing problem that occurs at low temperatures.

Table 1. Thermal properties of liquid TESMs in THS systems.

Material	Density [kg/m^3]	Specific Heat [kJ/(kg·k)]	Thermal Conductivity [W/(m·k)]	Thermal Capacity [J/(m^3·°C)]	Viscosity [Pa·s]
Water (20 °C) [40,41]	998	4.183	0.598	4174	-
Silicon Oil (Ak250) [40]	900–970	1.465	0.168	1421–2100	-
Transformer Oil (60 °C) [40]	842	2.090	0.122	1760	-
Therminol [24]	1056	1.575	0.135	1663	0.0030
Thermal Oil T55 [42]	766	2.455	0.11	1880	0.001021
Mineral Oil [41,43]	770–800	2.60	0.12	2080–2600	-
Synthetic Oil [41,43]	900	2.10–2.30	0.11	1890–2300	-
Rapeseed Oil [38]	781	3.385	0.217	2643	0.00291
Sunflower Oil [44]	915–920	1.863–2.439	0.139–0.163	1705–2232	0.057
Roki Oil [44]	909–950	1.888–2.404	0.153–0.170	1716–2280	0.08220
K-NaNO$_3$ (230 °C) [40]	1950	1.57	0.50	3062	-
Paraffin (20 °C) [40]	900	2.13	0.26	1917	-
Molten Salts [40,41]	500–2600	1.50	0.2–2.0	1350–3900	-
CaloriaHT 42 [45]	695	2.700	-	1877	-
Liquid Sodium (100 °C) [40]	927	1.385	85.84	1105	-

Table 2. The thermal properties of liquid TESMs with temperature variation.

Material	Thermal Properties	
Water [46]	Density [kg/m^3]	$739.57 + 1.9908T - 0.0038T^2$
	Specific Heat [J/(kg·k)]	$5438.6 - 8.07T + 0.0129T^2$
	Thermal Conductivity [W/(m·k)]	$-0.7888 + 0.0077T - 1 \times 10^{-5}T^2$
	Viscosity [Pa·s]	$0.0215 - 1.198 \times 10^{-4}T + 1.701 \times 10^{-7}T^2$
Solar Salt [18]	Density [kg/m^3]	$2089.9 - 0.6357T$
	Specific Heat [J/(kg·k)]	$1443.2 + 0.172T$
	Thermal Conductivity [W/(m·k)]	$0.443 + 1.9 \times 10^{-4}T$
	Viscosity [Ns·m^{-2}]	$22.714 - 0.12T + 2.281 \times 10^{-4}T^2 - 1.474 \times 10^{-7}T^3$
Hitex XL [47]	Density [kg/m^3]	$2240 - 0.827(T - 273.15)$
	Specific Heat [J/(kg·k)]	$1584 \pm 4.6\%$
	Thermal Conductivity [W/(m·k)]	0.519
	Viscosity [Pa·s]	$10^{6.1374}(T - 273.15)^{-3.36406}$
Jarysol Oil [29]	Density [kg/m^3]	$1261.569 - 0.7419173T$
	Specific Heat [J/(kg·k)]	$649.8400 + 3.187218T$
	Thermal Conductivity [W/(m·k)]	$0.1521663 - 8.240602 \times 10^{-5}T$
	Viscosity [Pa·s]	$e^{19.75102(\ln T)^4 - 492.2114(\ln T)^3 + 4602.0.9(\ln T)^2 - 19136.34\ln T + 29858.54}$

Solid TESMs encompass rocks [48], metals [38], ceramics [49], recycled materials [49], industrial waste [21], concrete [50], etc. Table 3 shows the thermal performance of various solid TESMs. When utilizing natural materials as TESMs, considerations should include their thermal and chemical stability. Grirate et al. conducted a comparative analysis of the thermal storage potential of six types of rocks (quartzite, basalt, granite, hornfels, cipolin, and marble) when used as filler materials for THS [51]. The research revealed that quartzite and cipolin stand out as the most suitable filler materials for a direct–packed bed THS system utilizing synthetic oil as the HTF. While basalt rock demonstrates superior thermal performance; its direct interaction with synthetic oil may induce corrosive phenomena, leading to diminished chemical compatibility.

According to different TES mechanisms, materials for THS can be divided into sensible and latent materials. Sensible TESMs, characterized by low cost and the ease of accessibility, have lower thermal storage capacities. Elouali et al. conducted a comparative study using four physical models on packed bed tanks employing different sensible heat materials [52].

Latent TESMs exhibit higher thermal storage capacities and stable working temperatures but are relatively expensive with lower thermal conductivity [53]. Various methods

have been developed to enhance the thermal conductivity of PCMs, such as mixing with high thermal conductivity nanoparticles [54], incorporating thermally conductive metals into PCMs [55], encapsulating PCMs in microcapsules [56], and installing fins on PCM tubes [57]. Microencapsulated PCMs are also effective in preventing PCM leakage and corrosion [56]. Ali et al. discussed in detail the latest progress of TES materials through multi-criteria decision technology and introduced the application of TES materials in construction, the industry, power, food storage, smart textiles, thermal management, and seawater desalination [58]. Nanomaterials and porous materials can greatly improve the thermal conductivity of phase change materials (up to 32%) and are most suitable for use in solar collectors and photovoltaic-based heat recovery systems [58,59].

Table 3. Thermal properties of solid TESMs in THS systems.

Material	Density [kg/m^3]	Specific Heat [kJ/(kg·k)]	Thermal Conductivity [W/(m·k)]	Thermal Capacity [J/(m^3·°C)]	Thermal Diffusivity [10^6 m^2/s]	Thermal Effusivity [10^{-3} × J/(m^{2}Ks$^{1/2}$)]
Alumina [29,38,49]	3600–4000	0.780–1.023	21–30	2810–4092	-	8.88
Alumina ceramics [39,60]	2200–3750	0.780–1.100	1.06–30.10	1716–2925	-	-
Aluminum [40,41,45]	2700	0.945–0.951	204–238.4	2419–2551	84.10–93.3	24.66
Basalt [51]	2210–3011	0.717–0.900	2–5.7	1750–2500	-	2.29
Bauxite [33]	3005	1.076	4.0	3233	-	3.59
Brick (dry) [40,45]	1500–1800	0.84–1.008	0.50	1417–1512	0.33	0.87
Ceramic [51,61,62]	2090–3120	0.837–1.076	3.982–17	1749–3357	-	1.52–2.37
Chalk brick [45]	3000	1.130	5.07	3390	1.9416	-
Cipolin [51]	2610–2870	0.800–1.470	3.2	1680–2520	-	-
Concrete [40,41,45]	2200	0.72–1.29	0.9–2.65	1680–3005	0.356–0.94	1.52
Copper [40,41,45]	8300–8960	0.385–0.419	372–385	3178–3729	107–112.3	35.97
Copper foam [39]	2700	0.800	126	2160	-	-
Gabbro [63,64]	2900–3500	0.710–0.980	2.19	2485–2842	-	-
Glue [62]	1730	1.0087	0.299	1745	-	-
Gneiss [65,66]	2590–2700	0.770–0.979	2.7–3.1	2008–2640	0.94–6.80	-
Granite [40,41,51]	2530–2750	0.600–12	2.2–2.9	1440–2880	1.18	2.67
Graphite [40,41]	2200–2400	0.61–0.660	30.40–155	882–1378	120	14.41
Hornfels [51,63]	2400–2800	0.700–0.900	1.5	2560–2880	-	-
High-temp concrete [39]	2750	0.916	1.0	2519	-	-
Iron [40]	7850	0.465	59.3	3348–6612	16.3	14.7
Lead [40,41]	11340	0.131	35.25	1485	23.6	7.24
Limestone [40,41]	2500	0.74–0.90	1.26–2.2	1584–2506	0.56–1.19	2.02
Magnesia [24]	1800	1.862	27.60	3352	-	-
Marble [45,51]	2560–2670	0.800–1.521	2.07–3.20	1680–2520	0.995–1.413	-
Mica [62]	2800	0.880	0.58	2464	-	-
Nichrome [62]	8400	0.460	16.75	3864	-	-
Pebbles [67]	1680	0.880	1.2	1479	-	-
Quartzite [42,51]	2320–2860	0.700–1.185	5.69–29.3	2002–3822	-	3.44
Quartz sand [62]	1730	1.2059	0.272	2086	-	-
Silicon carbide [39]	3210	0.750–1.043	9.01–120	2408–3348	-	-
Slag [40]	2700–2850	0.84–0.94	0.57–1.5	2268–2679	0.25	1.13
Sodium chloride [40]	2165	0.86	6.5	1836–1861	3.5	3.5
Sodium carbonate [41]	2510	1.090	-	2736	-	-
Soil (clay) [40]	1450	0.88	1.28	1276	1.0	1.28
Soil (gravelly) [40]	2040	1.84	0.59	3754	0.16	1.49
Stainless steel [49]	8030	0.50248	16	4035	-	-
Steel slag [68]	3430	0.877	1.47	3008	-	-

Yang and Cai conducted a comparative study on packed bed THS systems using sensible TESMs and PCMs as fillers, respectively, through experimental and numerical methods [69]. The research indicated that the total charging time for the THS system using latent TESMs was longer, and the TES capacity was greater compared to the system using sensible TESMs. The density and conductivity of sensible TESMs had a significant impact on temperature differentials, while reducing the melting point of PCMs decreased the total charging time, with the final TES capacity remaining unchanged. Canneto et al. characterized two ternary and quaternary strontium nitrate-based mixtures for THS [70]. They tested their thermophysical properties (melting temperature, specific heat, density,

viscosity, and thermal conductivity) and compared their storage performance with two commercial materials (solar salt and Hitec XL®). The simulation results indicated that both mixtures achieved higher discharging times. Lucio-Martin et al. experimentally assessed a hybrid THS tank consisting of a steel lining, an air gap interface, Calcium Aluminate Cement (a high-temperature concrete), and insulation materials (rockwool and expanded clay) [71]. Ternary molten salt and iron-rich waste were used as TESMs. The results demonstrated that the high-temperature concrete layer, serving as a suitable TESM and insulation, effectively withstood the thermal load during cyclic processes.

The development of TESMs using industrial by-products and recycled materials can significantly reduce material supply costs and address environmental impacts and issues related to raw material extraction and industrial waste disposal. This approach holds high environmental and economic value.

El Kouihen et al. systematically studied the potential application of a mining by-product (Porcellanite) as a TESM for recovering waste heat in mining operations [72]. They conducted comprehensive experimental characterizations, including chemical and structural composition, thermophysical properties, mechanical behavior, and durability testing. The study found that thermal treatment and cycling significantly improved the thermal performance of Porcellanite. The specific heat capacity of the cycled material was almost twice that of the raw material, and the tank integrated with Porcellanite achieved a charging efficiency of 87% and discharging efficiency of 88%.

Al-Azawii et al. experimentally compared the thermal performance of an innovative ceramic material, ReThink Seramic-Flora, made from recycled materials, and a commercial alumina-based TESM when filled in a THS packed bed and established a CFD model [73]. The cost of ReThink Seramic-Flora was expected to be 35–53% cheaper than commercial alumina. They found that ReThink Seramic-Flora and alumina exhibited similar performance in terms of net exergy efficiency. Subsequently, the research team used the CFD model from [73] to assess the cyclic thermal performance of a commercial-scale THS system filled with the two materials, considering dispersed thermal conductivity [49]. The simulation results showed that the net exergy efficiency of the Flora-filled thermal storage system increased from 72.5% to 88.6% over seven cycles, while alumina increased from 18.7% to 30.8%. Therefore, Flora was considered a superior TESM.

Modifying TESMs, by methods such as enhancing thermal conductivity [74], altering the melting point [75], increasing thermal storage density [76], and improving corrosion resistance [77], can directly enhance the thermal performance of THS systems. Lincu et al. increased the total heat capacity of a novel aluminum silicate by 36% through aluminum doping [78]. Nualsing et al. doped anodic aluminum into molten salt and observed that the charging time of the THS system containing 0.5 wt% anodic aluminum oxide was reduced from 3.75 h to 3.5 h [79]. Wang and Huang improved the thermal performance of steel slag through Na_2CO_3 activation [68]. The modified steel slag exhibited excellent thermal cycle stability, with a thermal energy storage density of 997.0 kJ·kg^{-1} (400–900 °C), representing a 25.3% increase over the original steel slag. The thermal conductivity at 25, 250, and 500 °C was 1.331, 1.323, and 0.889 W·(m·K)$^{-1}$, respectively, demonstrating a 32.7% improvement over the unmodified steel slag.

Liquid metals have attracted researchers' attention due to their excellent thermal conductivity. Wang and Han conducted a simulation study on the feasibility of using liquid lead–bismuth eutectic as an HTF in a packed bed THS tank, revealing its viability [80]. Wang et al. numerically investigated a THS tank filled with liquid sodium, evaluating and comparing five solid filling materials (quartzite, high-temperature concrete, copper foam, silicon carbide, and alumina ceramics) [39]. The results indicated that the addition of solid filling materials can enhance the discharge efficiency of the THS tank. Using high-temperature concrete provides optimal mechanical performance for the tank, and tanks employing alumina ceramics and high-temperature concrete both exhibit favorable operational performance.

Combining sensible TESMs and latent TESMs can leverage the characteristics of different materials, compensating for the performance deficiencies of individual materials and enhancing the performance of THS. Suresh and Saini developed an innovative combined sensible–latent THS system, employing concrete spheres as sensible TESMs and paraffin-encapsulated capsules as latent TESMs, and conducted experimental research [81]. The experimental results indicated that the novel combined sensible–latent THS system outperformed sensible THS systems, exhibiting better thermal performance with lower thermocline degradation during discharge and higher energy storage capacity and outlet temperature. The configuration employing multiple layers of different TESMs can be referred to as a cascaded layer configuration or cascade configuration. The volume percentages and filling sequence of different TESMs can influence the performance of THS, and these aspects will be discussed in detail in Section 5.

4. Application of Thermocline Heat Storage

Thermocline heat storage is primarily applied in renewable energy systems, with solar energy applications being the most extensively researched avenues. These include CSP plants, Parabolic Trough Power (PTP) plants [18], domestic hot water applications [82], solar cooking systems [83], solar air heaters [35], and the solar cogeneration of power [24]. THS can also be integrated with various energy storage systems such as adiabatic compressed air energy storage [84], liquid air energy storage [85], and Pumped Thermal Energy Storage (PTES) [86]. Additionally, THS finds applications in biomass power plants [87], waste heat recovery [88], space heating and cooling for individual buildings and communities, and heat pump systems [85,89].

Combining THS with solar energy applications can mitigate the intermittent nature of solar energy, enhance effective working hours and stability, and reduce overall system costs. Petrollese et al. proposed and studied a novel PTES system integrated with CSP plants, consisting of a storage system with three packed bed THS tanks and argon as the working fluid [90]. A mathematical model was developed to simulate the CSP-PTES system, analyzing the thermal behavior of the THS tanks and evaluating the required storage capacity. In subsequent research [37], the team optimized the design of the CSP-PTES system, using granite rock as the solid TESM for the TES system, and formulated control strategies based on power demand, weather conditions, and system performance levels. Chekifi and Boukraa provided a descriptive review and critical analysis of THS in CSP plants [45].

Ingenhoven et al. combined a high-temperature packed bed THS system with a solar expanding-vortex particle receiver (SEVR) to store the heat generated by the SEVR's high-temperature air [34]. In a subsequent study [32], they established a transient model for the thermal–economic analysis and optimization of the entire system, emphasizing the coupling between various system components. Pradeep and Reddy proposed integrating THS with the solar cogeneration of power and desalination, developing a detailed mathematical model to study the impact of factors such as TESMs, porosity, and tank height on system performance [24]. Additionally, economic and environmental analyses were conducted for this combined system. The results showed that the TES system significantly reduced the payback period of electricity costs from 4.61 years to 2.31 years, and the annual reduction in carbon dioxide pollutants was 92.95 metric tons.

The integration of THS with certain household facilities can leverage its attributes of its simple structure and cost-effectiveness, thereby reducing residential energy costs and enhancing the quality of life in underdeveloped regions. Chandra and Matuska conducted a comprehensive review of the stratification in domestic hot water storage tanks, considering thermal stratification models, flow models, and various parameters affecting tank performance [91]. Zhou et al. compared the annual performance and economic viability of a solar cooking system integrating a THS unit and a dual-tank storage unit [42]. The study investigated system configurations, including the solar collector area, thermal storage days, and tank heat loss coefficient. The research suggested that a THS solar

cooking system filled with natural quartzite exhibited the longest continuous operation period throughout the year and was the most economical. Compared to electric and gas cooking systems, it can save 1.75 tons and 0.52 tons of carbon emissions annually.

Additionally, some researchers have reported novel applications of THS. Gaggioli et al. conducted an experimental verification of an integrated system comprising a THS tank and a steam generator [92]. The results indicated that, compared to traditional dual-tank and external steam generator systems, the new system offered greater economic efficiency and operational convenience. Tiwari and Sharma integrated a THS system into a metal hydride reactor and developed a three-dimensional model to analyze the effect of gas supply pressure on reactor performance [93]. The results showed that when the supply pressure was 16 bar, the thermocline energy storage system successfully stored the energy generated inside the metal hydride reactor, with a storage efficiency of 81.7%. The discharge efficiency of the desorption process exceeded 70%. A schematic diagram of the integration of the metal hydride reactor and THS reactor is shown in Figure 4.
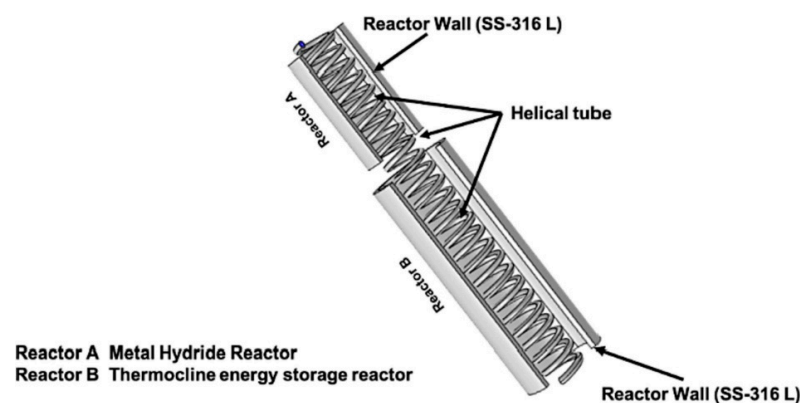
Figure 4. Schematic of metal hydride reactor integrated with THS reactor [93].

Schwarzmayr et al. investigated the integration of packed bed THS and waste heat recovery in the steel industry and evaluated the applicability and robustness of gas powder two-phase exhaust gas as an HTF [88]. The experimental results showed that approximately 98% of the powder accumulated in the packed bed during the charging process. Reversing the flow direction of the HTF did not reduce the powder retention in the packed bed, and the thermal storage system also acted as a dust collector. During the charging process, the pressure drop in this energy storage system exponentially increased, leading to a decrease in the system's exergy efficiency and potential bed blockages. Hence, the regular maintenance and cleaning of the packed bed were required. A further assessment of the long-term stability of this system in operation is needed, along with the development of new structures to simplify maintenance and cleaning procedures. This study provides valuable insights for enhancing the environmental benefits of THS systems and expanding their applications, warranting further investigation.

5. Optimization of Thermocline Heat Storage

This chapter provides a comprehensive review and organization of research on the optimization of THS. Through a literature analysis, recent studies can be categorized into three main types: the optimization of the design of THS systems, optimization of the thermal heat storage process and operational strategies, and development and optimization of numerical models for THS.

5.1. Optimization of Thermocline Heat Storage System Design

The design of the THS system includes the structural design of the THS tank and the arrangement of solid TES materials inside the tank. The optimization of THS system design aims to enhance the thermal performance of the system under specific conditions while meeting economic and environmental requirements.

5.1.1. Tank Structure

The structural design of THS tanks includes considerations such as tank shape, aspect ratio, inlet/outlet configurations, and the flow direction of the HTF. For indirect THS tanks, the design must also account for the heat exchanger [82] or immersed coil.

Tank Shape

In the majority of THS systems, cylindrical tanks are commonly employed due to their simple structure, uniform stress distribution, and a favorable ratio of volume to surface area compared to cubic structures. Numerous studies have compared and optimized tank shapes using numerical methods. Figure 5 shows some recent studies on the shape of storage tanks, including models and the experimental setup.

(A)

(B)

(C)

(D)
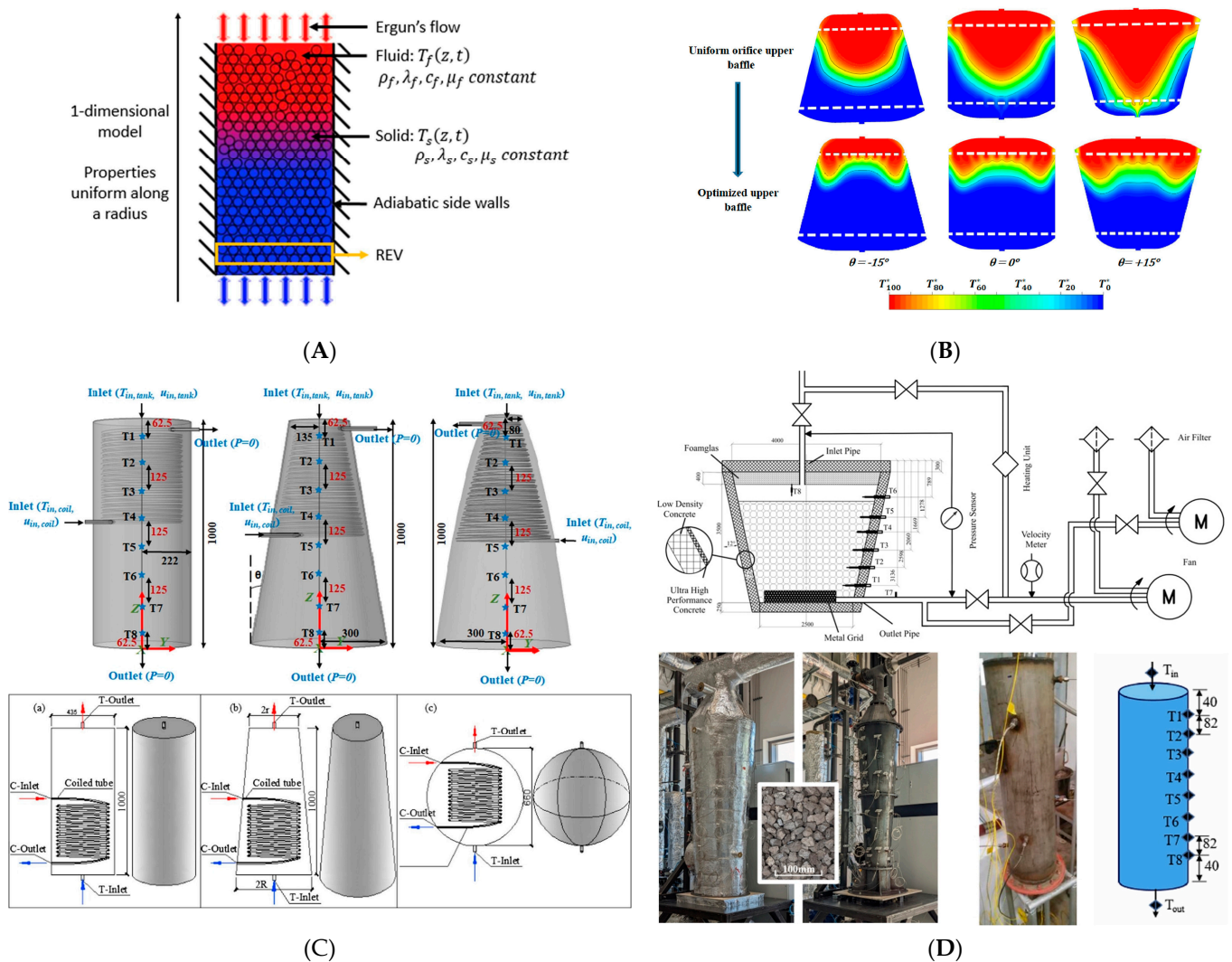
Figure 5. Models and experimental setups for the research of THS tank shape in recent literature: (**A**) 1D model; (**B**) 2D model; (**C**) 3D models; and (**D**) experimental setups [94–100].

In studies such as [27,94,101], researchers conducted Computational Fluid Dynamics (CFD) simulations to compare the performance of tanks with different shapes. Yang et al. investigated the thermal storage performance of 10 different shapes (Cylinder, Sphere, Cone, Truncated cone, Ellipsoid, Spindle, Barrel, Cylinder + sphere, Cylinder + truncated cone, Cylinder + cone) in a static operating mode (as shown in Figure 6) [101]. The study revealed a strong positive correlation between the ratio of the tank volume to surface area and thermal and exergy efficiency, as the exergy losses of the tank were mainly caused by heat losses to the environment. Consequently, spherical tanks exhibited the highest

efficiency, followed by barrel-shaped tanks, while cylindrical tanks showed the lowest efficiency. Tanks with sharp angles exhibited higher thermal stratification, while those with flat surfaces showed lower thermal stratification.
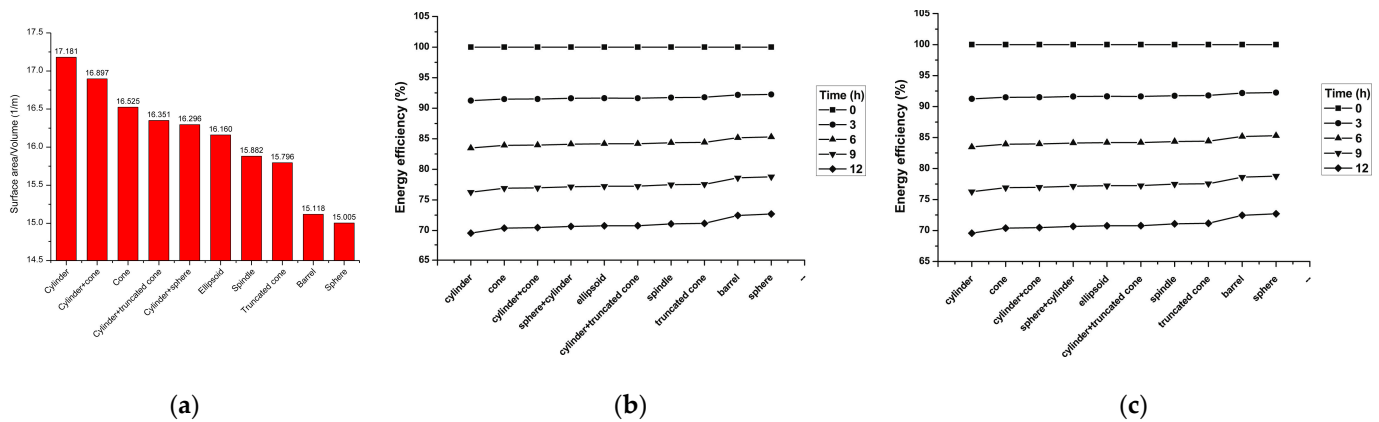

Figure 6. A performance comparison of storage tanks with different shapes. (**a**) The ratios of the surface area to volume with different water tank shapes. (**b**) Variation in the thermal energy storage efficiencies of different shapes over time. (**c**) Variation in the thermal exergy storage efficiencies of different shapes over time [101].

Li et al. investigated the thermal storage characteristics of three shapes (cylindrical, circular truncated conical, spherical) of indirect water tanks with the same volume [94]. The circular truncated cone tank demonstrated the highest temperature stratification and charging efficiency, while the spherical tank exhibited the poorest performance. For circular truncated cone tanks, as the radius ratio (ratio of upper surface radius to lower surface radius) decreased, the temperature stratification within the tank became more pronounced, albeit with lower charging efficiency. Two-dimensional CFD simulations by Lou et al. indicated that a circular truncated cone SMTHS tank with a positive cone angle (larger upper diameter than lower diameter) was optimal during the charging process [95].

Khurana et al. used a two-dimensional unsteady model to study the thermal performance of SMTHS tanks with cylindrical, conical, and parabolic shapes [97]. The study found that compared to conical and cylindrical tanks, the parabolic shape had lower convective heat losses and higher thermal efficiency. The research group further used a three-dimensional numerical model to study the thermal performance of indirect SMTHS tanks with different geometric shapes [96]. Evaluations based on insulation, energy utilization, and entropy generation indicated better performance for the parabolic shape. Kurşun and Burak numerically investigated the influence of tilt angle and aspect ratio on rectangular water tanks [102]. They found that inclined placement weakened the fluid movement caused by natural convection within the rectangular tank, enhancing thermal stratification.

Schwarzmayr et al. conducted experimental research on a conical packed bed tank [98]. Ortega-Fernández compared the cylindrical and conical geometries of packed bed tank bodies, concluding that cylindrical tank bodies could store more energy and had higher thermal performance [27]. Zanganeh et al. used a truncated conical storage tank immersed in the ground in an experiment on a pilot-scale packed bed THS system applied to CSP power plants [99]. This design aimed to reduce the normal forces on the tank walls. Subsequently, they numerically studied the cyclic performance of the tank, finding that, under the same operating conditions, the truncated conical tank required a smaller height and volume to extract energy from the airflow. This was attributed to the larger top diameter of the conical tank, allowing it to store more energy at the top. During the initial charging stage, the truncated conical tank exhibited a larger pressure drop, which decreased as charging progressed, as the average temperature inside the cylindrical tank was higher, resulting in a larger pressure drop than in the truncated conical tank.

In the literature [103], for packed bed tanks with the same height and volume, reducing the top diameter of a negative cone-shaped tank resulted in smaller wall losses, higher discharge temperatures, and increased exergy efficiency but required the additional consideration of the thermal ratchet problem. Le Roux et al. optimized a packed bed THS system using a particle swarm optimization algorithm, combining exergy and LCA [100]. As the exergy weight increased, the tank shape transitioned from square to tapered.

Through the literature review, it is evident that different tank types exhibit significant differences in thermal performance under different operating modes. For packed bed tanks, truncated cone tanks with positive cone angles demonstrate better overall performance. In charging mode, SMTHS tanks with a parabolic shape exhibit superior performance. For tanks requiring long-term standby modes, spherical or barrel-shaped tanks should be employed.

Aspect Ratio

The aspect ratio is the ratio of the height to the diameter of a storage tank. For tanks with the same diameter, as the height of the tank increases, the aspect ratio also increases. In the case of cylindrical THS tanks, some studies suggest that increasing the aspect ratio can result in a thinner thermal stratification layer, leading to improved thermal stratification [31,104,105]. Increasing the height of the tank can enhance the exergy efficiency, but it also comes with an increase in material costs [103]. During the charging process, THS tanks with lower aspect ratios exhibit higher charging efficiency, while during the discharging phase, higher aspect ratios contribute to improved discharging efficiency [104]. Bai et al. conducted a study on the thermal stratification of cylindrical SMTHS tanks with different aspect ratios using a 2D model [106]. The results indicated that a tank with an aspect ratio of 1:1 achieved the highest energy and volumetric efficiency in standby mode. For $H/D < 3$, increasing the aspect ratio would lead to more pronounced thermal stratification, whereas for $H/D > 3$, the aspect ratio had a minimal impact on thermal stratification.

Increasing the aspect ratio also results in higher pressure losses within the THS tank, affecting the overall system efficiency. Skuntz et al. investigated the influence of aspect ratio on the efficiency of axial and radial flow packed bed THS tanks [107]. For axial flow tanks, thermal efficiency and pump power increased with the aspect ratio, resulting in a peak net efficiency before declining. In contrast, for radial flow tanks, thermal efficiency and pump power decreased with the aspect ratio, also leading to a peak net efficiency before decreasing. The optimal aspect ratio for packed bed tanks depends on the size of the packing particles, with total exergy losses decreasing initially and then increasing with the aspect ratio [31]. Due to heat dissipation losses, designs with low aspect ratios are not particularly suitable for long-term storage, such as monthly or seasonal storage.

For parabolic and conical tanks, an increase in aspect ratio leads to a thicker initial thermocline zone and increased energy losses, resulting in the degradation of thermal stratification [97]. In the case of rectangular tanks, an increase in aspect ratio enhances thermal stratification, leading to improved thermal storage efficiency [103]. Constructing tall tanks with high aspect ratios introduces mechanical complexity and thermal ratchet risks [27]. Due to mechanical constraints, the maximum height of packed bed tanks is limited to approximately 16 m [108]. In summary, under specific design conditions, storage tanks should have an optimal aspect ratio.

Inlet and Outlet Configuration

In the process of charging and discharging in a THS tank, the inlet jet flow causes disturbances to the water and temperature field in the tank. Lou et al. utilized CFD simulations and Particle Image Velocimetry systems to investigate the flow patterns of the inlet thermal jet in an SMTHS tank [109]. They visually demonstrated the impact of jet entrainment on the thermocline and temperature stratification.

In existing studies, there are two methods to overcome the disturbances caused by the inlet jet to water and thermal stratification. One is to optimize the shape of the tank's inlet and outlet (Figure 7), and the other is to use flow diffusers (distributors) to distribute the high-momentum main inflowing jet into multiple sub-flows, forming radial or reverse flow to mitigate disturbances [110] (Figure 8).
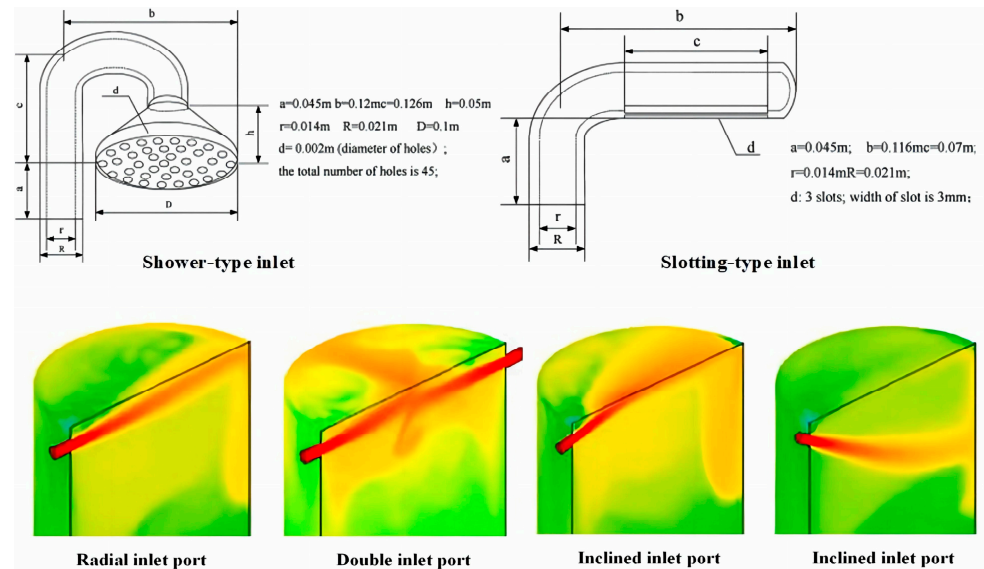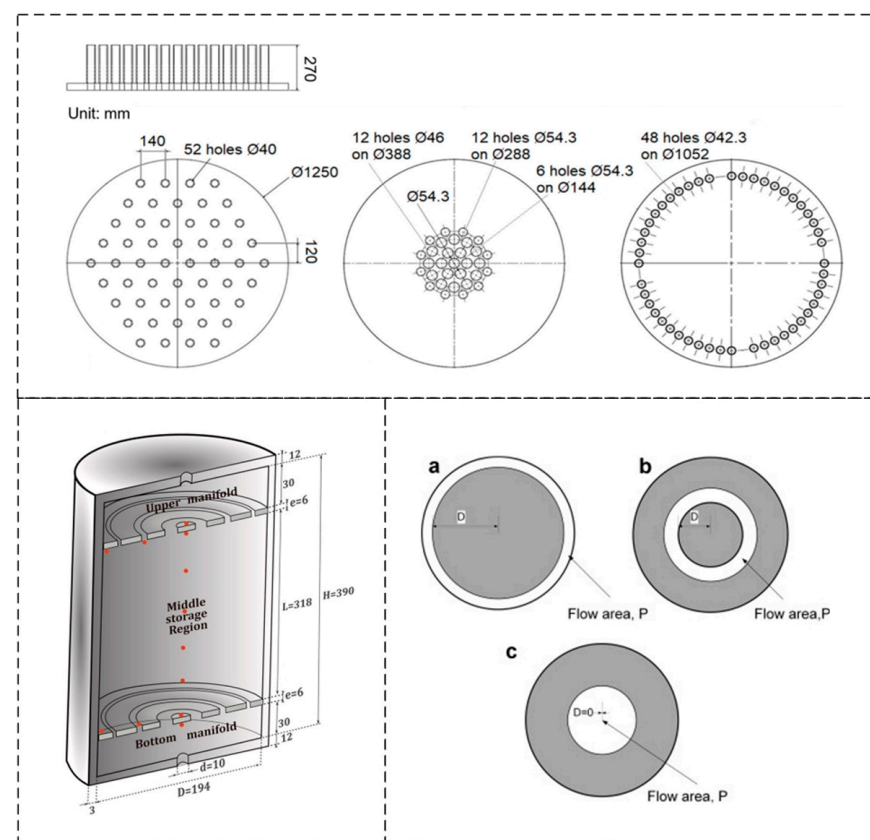

Figure 7. Different inlet types [111,112].

Figure 8. Different flow distributors, (a–c) represent different radial non-uniformity [46,110,113].

Shafieian et al. conducted a 3D unsteady CFD simulation to study the influence of different inlet geometries (double inlet, diffuser, inclination) on the thermal stratification

in SMTHS tanks [112]. The simulation results showed that the tank with a double-inlet structure had better thermal stratification at high flow rates. Diffusers with length-to-width ratios between 1.0 and 1.5 positively influenced thermal stratification, while the inlet angle had minimal impact on the overall temperature distribution. For rectangular SMTHS tanks, slotting-type inlet tanks exhibited higher effective discharge efficiency and effective discharge time compared to direct inlet tanks and shower-type inlet tanks [111]. Shaikh et al. reported that in SMTHS tanks, the thickness of the thermocline zone for tanks with axial inlets was smaller than that for tanks with radial inlets [105]. Lou et al. optimized SMTHS tanks by inserting perforated baffles in the inlet/outlet manifolds and developed an innovative optimization algorithm for optimizing the distribution of holes on the baffles [95]. The numerical simulation results showed that the optimized structure created a quasi-thermal piston flow in the tank, resulting in the best thermal stratification. Compared to the unoptimized structure, the efficiency of fully charging the tank increased by 29%. Subsequently, the team proposed a new distributor called Ring-Opening Plate Distributors (ROPDs) and used the optimization algorithm from [95] to optimize the size distribution of the circular openings [46]. This increased the charging and discharging efficiency of laboratory-scale SMTHS tanks by 14.5% and 19.8%, respectively. The overall efficiency increased from 56.3% to 84.2% compared to simple inlet/outlet configurations.

Vannerem et al. experimentally studied the effects of three inlet fluid distributions (uniform fluid distribution, central distribution, and peripheral distribution) on the performance of packed bed THS [113]. The results indicated that, due to the buffering effect of solid fillers, fluid distribution had less impact on the performance of semi-industrial-scale packed bed thermocline storage. Chen et al. developed a three-dimensional transient model to study the influence of annular distributor gaps on the charging and discharging processes of SMTHS tanks [38]. The simulation results showed that the distributor gap did not significantly affect the temperature curve trend during discharging, meaning it did not have a significant impact on heat exchange inside the tank. It primarily influenced the uniformity of the flow field, with the thermal storage efficiency increasing with larger distributor gaps. The discharge efficiency decreased first and then increased, reaching the lowest value of 72.8% at a gap of 50 mm and increasing to 75.8% at a gap of 80 mm. Bellenot studied the influence of fluid distribution on the thermal–hydraulic behavior of SMTHS tanks through experiments and numerical methods [114]. The results suggested that under certain conditions, the efficiency of strong axial injection was slightly higher than that of uniform injection because non-uniform injection could locally accelerate the fluid, thereby improving heat exchange with solids and limiting the thickening of the thermal gradient. However, overall, the impact of fluid distribution on system performance was minimal. During the discharging process, axial collectors with high injection effects collected more energy than smaller-diameter radial collectors.

In the case of the upward flow of the HTF through a packed bed THS tank, solid particles usually remain stationary, referred to as the fixed bed regime. For high flow rates and small particle sizes, the forces exerted by the fluid on the particles balance their gravity, leading to what is known as the incipiently fluidized bed. The fluid velocity at this stage is called the minimum fluidization velocity of the solid particles. When the fluid velocity exceeds the minimum fluidization velocity of the solid particles, it causes the bed to become unstable, resulting in fluid bubbles, known as a bubbling fluidized bed [115]. The high mixing of solids in a bubbling fluidized bed leads to uniform temperature throughout the operation, significantly reducing the thermal storage performance of packed bed tanks [116,117].

Cano-Pleite et al. proposed a novel confined bed, mechanically limiting particle materials through two fluid distributors at the bottom and top of the bed to maintain a fixed bed regime [118]. They conducted a thermal–economic optimization of the novel THS system by analyzing models, finding that the optimal size of the constrained bed largely depended on the particle material's particle size. Depending on the different thermal storage demand times, the bed aspect ratios ranged from 0.25 to 0.9. Subsequently, the research team

conducted experimental studies on this novel confined bed THS system, confirming the confinement of the distributor on particles and demonstrating good consistency between experimental and numerical predicted values [119]. Figure 9 shows the experimental setup of a confined bed and a fluidized bed.
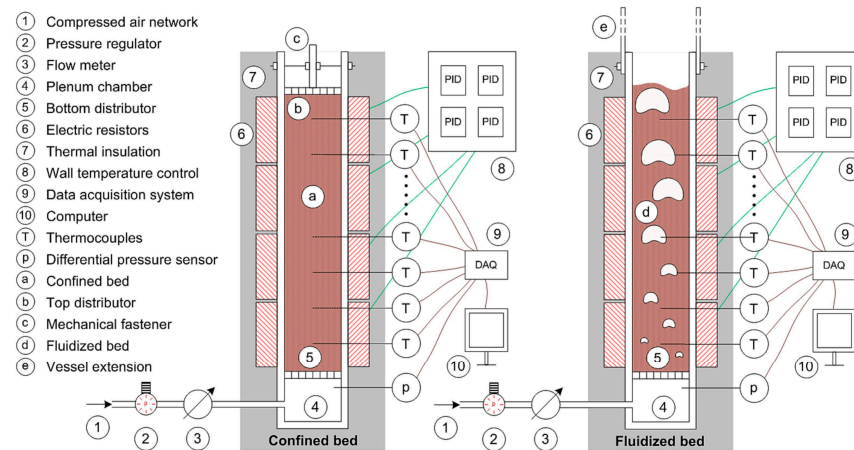

Figure 9. The experimental setup for a confined bed and a fluidized bed [119].

Flow Direction

The flow direction of the HTF within the THS tank can be categorized into axial and radial flow. McTigue and White developed a thermodynamic model for a packed bed THS tank with the radial flow of the HTF. They optimized the system using a multi-objective algorithm and compared the thermal–economic performance with a similarly sized tank employing axial flow [120]. The results indicated that the radial geometry influenced velocity profile and thermocline shape, achieving lower pressure losses but resulting in steeper temperature peaks, leading to increased heat and conduction losses. The schematic diagram of the charging process of the radial flow packed bed is shown in Figure 10.
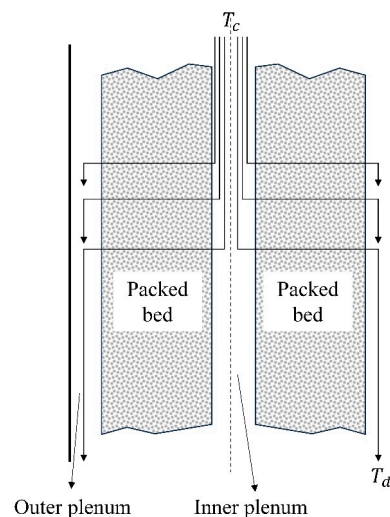
Figure 10. A schematic of a radial flow packed bed during charge.

Daschner et al. conducted experimental tests on a pebble heater with radial fluid flow, which can serve as a TES to simultaneously realize electricity-driven operation for biomass power plants and reliable heating, with a thermal efficiency of approximately 92% [87]. Skuntz et al. numerically performed a detailed comparison between radial and axial flow packed bed THS tanks [107]. As the aspect ratio of the radial flow bed increased, the diffusion of the thermal peak rose and pressure drop decreased, exhibiting the opposite

trend in the axial flow bed. The net efficiency range for radial flow was from 74% to 82%, while axial flow ranged from 80% to 87%.

Radial flow packed bed configurations possess inherent insulation as the outlet fluid channels are located on the outer side of the tank, near the tank wall where temperatures are low. It is worth noting that a challenge associated with radial flow configurations is the thermo-mechanical stress caused by the radial temperature gradient: particles near the center are hotter and expand more than adjacent particles, resulting in stress.

Heat Exchanger Configuration

For the indirect THS system, also known as a closed system, the HTF in the external system does not directly contact the thermal storage medium inside the TES tank. Instead, heat exchange is facilitated through a heat exchanger or coil. The configuration of the heat exchange components has a decisive impact on the efficiency of the indirect THS system.

Cagnoli et al. established and validated a transient 2D CFD model for an indirect SMTHS tank, equipped with two flat tube heat exchangers [47]. The simulation results for the tank's charging and discharging processes indicated that the bypass in the heat exchanger position significantly reduced the thermal performance of the THS system. Therefore, optimizing the tank structure is crucial to enhance the flowability of the HTF inside the tank. In an indirect THS system, the outlet temperature is higher when the immersed heat exchanger is at its highest position [26].

The "CSP Research Group" at ENEA developed an indirect SMTHS tank, comprising two helical heat exchangers immersed in the HTF and two isolated channels to promote natural circulation within the tank and accelerate the formation of the thermocline zone. Capocelli et al. tested a prototype of this concept and validated a simplified heat exchange model through experimental results, replicating the heat performance of heat exchangers inside the tank [121]. The schematic diagram of the prototype is shown in Figure 11. In subsequent work, the research group developed and validated a new ad hoc model to simulate the charging and discharging processes of the tank [122]. They proposed an analytical solution capable of assessing the thermocline distribution based on time and radius.
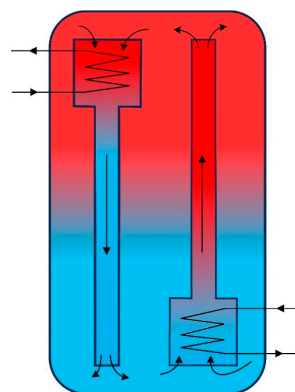

Figure 11. A schematic of the THS tank prototype realized by ENEA.

5.1.2. Arrangement of Solid Thermal Energy Storage Materials

According to the arrangement of solid TESMs, the DMTHS storage tank can be divided into a packed bed tank and structured tank. In packed bed tanks, solid TES particles are only constrained by the tank walls and densely pile up due to gravitational forces, while in structured tanks, solid TESMs are arranged in accordance with a specific design pattern.

In the structure of packed bed tanks, the disordered packing method is simple in structure and cost-effective, making it the most widely used filling method [123]. However, the pressure drop in a disordered packed bed is usually high [124], and the uneven distribution of TESM particles can lead to non-uniform fluid flow and heat transfer [125]. Optimizing the packing method and particle size of TESM particles can improve the performance

of THS systems. The current primary optimization methods for TESM particle packing include three configurations, with their characteristics summarized in Table 4, which will be further elaborated in the subsequent sections.

Table 4. Optimized packing methods and their characteristics.

Reference	Optimized Packing Method	Description	Characteristics
[112,113]	Ordered packing	Filled with TESM particles in a certain order	The pressure drop in ordered packing is lower than that of disordered packing, and the temperature field is more uniform. Multi-layered ordered packing with particles of different sizes is superior to single-layered ordered packing because it can effectively shorten charging time and reduce thermocline degradation.
[45,114–119]	Cascaded configuration	Filled with multiple layers of different TESM particles	Matching the thermal properties of TESMs with the HTF temperature curve along the bed gives the cascade configuration better thermal performance and higher overall efficiency than the single-layer configuration and shortens the charging time. Among multiple cascade configurations, the sensible–latent heat hybrid cascade configuration has higher charging and discharging efficiency and utilization rate. It is economical to replace some PCMs with sensible TESMs.
[21,42,49,120–123]	Structured configuration	Arrange TESMs in a certain shape or pattern in the THS tank	Avoiding the risk of thermal ratcheting and solving the problem of excessive pressure drop in packed bed configurations under high flow rates. Compared to the packed bed configuration, the capacity cost of the structured configuration is lower, but the efficiency is also slightly reduced.

Ordered Packing Configuration

Zhang et al. numerically studied the thermal storage performance of packed beds in three different packing models (strip packing model, in-line packing model, and disordered packing model) [126]. The results showed that the temperature field uniformity of the ordered packing model was significantly better than that of the disordered packing model. In addition, compared with strip packing, in-line packing had obvious advantages in energy efficiency and thermal storage capacity. Lv et al., using finite element methods, studied the impact of PCM microcapsule packing methods on the thermal performance of packed bed THS systems, investigating single-layered, diameter-changed two-layered, and three-layered packing models [127]. The results indicated that adopting cross-packing methods can improve the charging process, and multi-layered systems exhibit better thermal storage performance than single-layered systems, manifested by reduced charging times and less degradation of the thermocline.

Cascaded Configuration

Due to the axial temperature distribution differences in the THS tank, different materials can be used to fill the upper, middle, and bottom parts of the tank to leverage their respective thermal properties. This configuration, composed of multiple layers of different TESMs, is known as a cascaded configuration or cascaded layers configuration. Cascaded configurations exhibit higher thermal characteristics and overall efficiency compared to single-layered structures [53,128], and they reduce charging times [129].

Cheng and Zhai experimentally validated a simulation model of a cascaded THS tank filled with different PCMs, analyzing the thermal performance of uniformly distributed multi-stage cascaded THS tanks, with the highest number of stages reaching 24 [129]. The simulation results showed that the charging time of a 24-stage configuration is 15.1% less than that of a single-stage configuration. Considering cost and structural factors, a recommendation was made for three–five stages.

Elfeky et al. conducted multiple studies on cascaded tanks. In 2018, the research group developed a transient Concentric–Dispersion numerical model to study the dynamic performance of a cascaded THS tank filled with PCM capsules [130]. The numerical results showed that during charge–discharge cycles, the melting temperature variation in three-stage PCMs matched the HTF temperature curve along the bed layer, significantly enhancing the heat transfer rate and overall efficiency of the THS system. Subsequently, they proposed optimizing the latent heat and melting temperature values of multi-stage PCM configurations through dimensionless temperature and inverse Stefan number to improve the overall efficiency of the THS system during charge–discharge cycles [131]. The optimization results indicated that the melting point of the top phase change stage should be lower than the HTF inlet temperature, while the melting point of the bottom phase change stage should be higher than the HTF outlet temperature. In 2022, the research group numerically studied the thermal and economic performance of a mixed sensible–latent THS tank. The mixed tank had encapsulated PCM thin stages at the top and bottom and sensible TESMs in the middle [53]. Seven configurations were designed based on different PCM stage thicknesses and compared with a pure sensible THS tank. The results indicated that the thermal performance of the mixed tank was superior to the sensible heat configuration. In their recent research, they compared the performance characteristics of mixed sensible–latent heat storage and cascaded latent heat storage under different operating conditions using two mathematical models. They found that, for different charging times, the total efficiency and utilization rate of the mixed sensible–latent heat tank were higher than the cascaded latent heat tank [132]. During charge–discharge operations, the solidification of PCMs at high temperatures increased the heat transfer rate of the fluid and PCM capsules, and raising the melting temperature of the top PCM could enhance the overall efficiency during the charge–discharge phase [18].

Elsihy et al. evaluated the effect of different volume fractions of sensible TESMs and PCMs on cyclic behavior in a hybrid sensible–latent THS system and compared four cases, with case 4 having the maximum heat storage capacity and maximum capacity ratio and case 2 having the highest utilization rate [133]. The hybrid sensible–latent THS system with four configurations is shown in Figure 12.
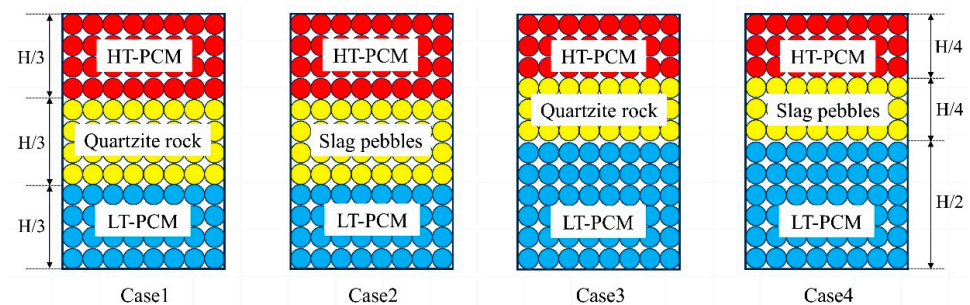

Figure 12. Four cases of hybrid sensible–latent THS system.

Structured Configuration

The structured configuration has two main advantages: one is that it will not have a mechanical effect on the tank wall due to the expansion and shrinkage of solid TESMs during the thermal cycle, which can avoid the risk of thermal ratchet; the other is to solve the problem of the excessive pressure drop in the packed bed tank at a high flow rate [45]. There are three forms of structured tanks: arranging solid sensible TESMs into bricks and stacking them orderly inside the tank [134,135]; molding solid sensible TESMs (concrete) into prisms or flat plates and embedding them in the tank [50,136]; and orderly packing solid TESM particles into channels formed by grating inside the tank [137].

A comparative study indicates that the efficiency of packed bed tanks is approximately 8.5% higher than that of structured tanks, with a capacity cost more than 12% lower for the latter [136]. Motte et al. proposed a mathematical model to study the thermal behavior

of structured tanks filled with ceramic bricks, revealing lower convective heat transfer between the structured filling material and the HTF [21,135].

Wu et al. compared the thermal performance of structured THS tanks with different solid filler distribution structures [50]. They investigated the influence of characteristic dimensions and inlet flow velocity on system performance, considering four concrete structures: the channel-embedded structure, the parallel-plate structure, the rod-bundle structure, and the packed bed structure. The study showed that the heat exchange rate between concrete and fluid in the packed bed structure is the fastest, resulting in the highest discharge efficiency and longest effective discharge time, while the channel-embedded structure has the lowest discharge performance. Figure 13 shows a schematic diagram of the cross-section of THS tanks with different concrete structures.
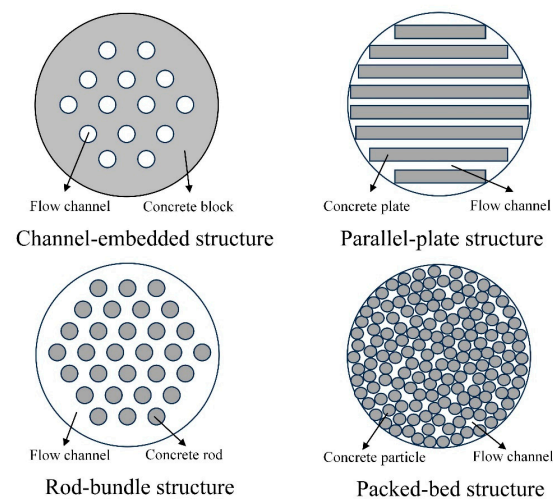
Figure 13. A schematic of the cross sections of the THS tanks with different concrete structures.

Yu et al. proposed a structured THS device and established a mathematical model to investigate the thermal–hydrodynamic characteristics for the charging process of this unit [137]. The device, divided into several channels by grating, features orderly packed PCM capsules within the channels. The schematic of the horizontal SPLTES unit with PCM capsules is shown in Figure 14.
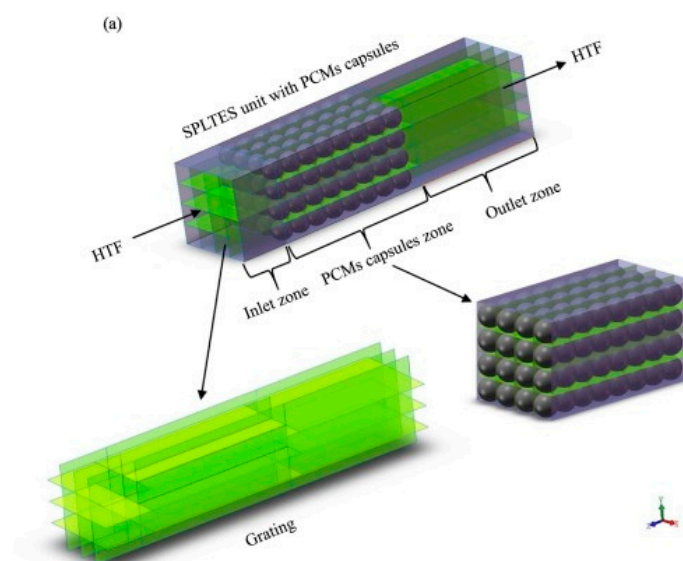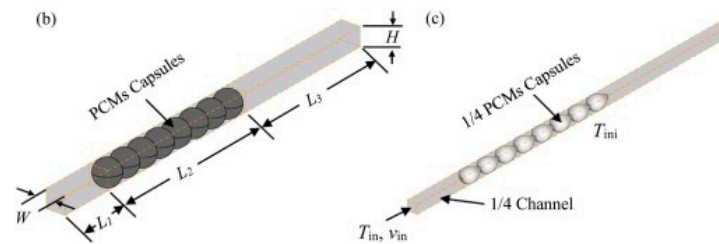

Figure 14. *Cont.*

Figure 14. A schematic of the horizontal SPLTES unit with PCM capsules. (**a**) SPLTES unit; (**b**) geometry of one channel in the SPLTES unit; (**c**) computational domain [137].

Zahid et al. introduced a structured hybrid sensible–latent THS tank, consisting of upper and lower layers of copper pipe-encapsulated PCMs, separated by structured concrete blocks [57]. Experimental comparisons were made among four configurations of THS tanks: multi-layered sensible heat concrete with PCMs (MLSPCM), two uni-layered sensible concrete with PCMs (SLSPCM-1 and SLSPCM-2), and single sensible heat concrete block (SSCB), demonstrating that the MLSPCM configuration has the highest energy storage capacity and charging–discharging efficiency.

Particle Diameter

Changes in particle diameter affect the convective heat transfer between particles and the HTF, internal heat conduction within particles, and the pressure drop in packed bed tanks, thereby influencing the overall efficiency of the THS system. As particle size increases, the temperature difference between the center and surface of the particles increases, reducing the heat transfer area between particles and the HTF, resulting in a decrease in exergy efficiency. Simultaneously, pressure drop decreases with increasing particle size, reducing pump power and increasing exergy efficiency [103]. Decreasing particle size reduces the thickness of the thermocline zone, reducing charging time [138] and increasing effective discharge time [139]. For cross-packing, reducing particle size can cause pressure drop to increase dramatically, up to 16 times [127]. Therefore, both excessively large and small particle diameters lead to a rapid decline in efficiency.

For different packed bed tank configurations, the influence of particle size on THS thermal performance varies, and each configuration corresponds to a different optimal particle size. The authors of Ref. [139] reported that for different materials, when the particle size increases by 25 times, the effective discharge efficiency of the system decreases by 23–39%. In some cases, decreasing particle size reduces overall energy storage efficiency [27,31]. In a study by the authors of [137], reducing the diameter of PCM capsules significantly shortened the charging process of structured THS devices. When the diameter of PCM capsules increased from 8 mm to 16 mm and 24 mm, charging time increased by 391.4% and 884.4%, respectively, with little impact on total heat storage capacity. The authors of Ref. [27] proposed that the optimal efficiency and thermal performance can be achieved with particle diameters around 10 mm, while the multi-objective optimization results in [103] showed that the highest efficiency design had a particle diameter of 21.5 mm. In [104], the effect of particle size variation on efficiency was minimal.

It should also be noted that the normalized stress of packed bed tanks increases with increasing filler particle size [20]. Therefore, smaller filler particle diameters will improve the mechanical performance of the thermocline tank.

5.2. Optimization of Operating Strategies for Thermocline Heat Storage Systems

Clarifying the impact of process parameters, such as flow velocity and temperature, as well as the charging and discharging strategies during the operation of THS systems is crucial for enhancing efficiency and stability. Furthermore, this understanding allows for the rational design of THS systems based on specific parameter requirements.

5.2.1. Flow Velocity

Numerous studies have investigated the influence of flow velocity on THS systems. An increase in flow velocity often causes an augmentation in thermocline thickness, thermal stratification degradation, and the percentage of thickness increase can reach 228% [20,57,97,138]. However, the impact of flow velocity on the efficiency of THS systems is complex and varies according to the type of THS system.

For SMTHS tanks, lower flow velocities lead to smaller initial thermocline thicknesses. As charging progresses, the thermocline thickness expands, and the difference in thickness caused by various flow velocities depends on the initial thickness [16]. Increasing inlet flow velocity induces more fluid mixing, enhancing heat transfer on one hand and increasing disturbance to the thermocline on the other. To achieve optimal design, the effects of both mixing and heat diffusion should be considered simultaneously [112]. Under the same configuration, a higher Reynolds number results in lower efficiency for SMTHS tanks [95]. Excessive flow velocities ($Re_{tank} > 167$) in SMTHS tanks lead to a sharp decrease in charging and discharging efficiency, and the use of distributors mitigates the degradation in performance caused by high flow velocities [46].

In DMTHS tanks with porous media flow, the flow regime can be determined based on the Reynolds number (Re_p) of the particle size: (a) Darcy or creeping flow regime ($Re_p < 1$), (b) Forchheimer flow regime ($1 < Re_p < 150$), (c) post-Forchheimer flow regime (unsteady laminar flow, $150 < Re_p < 300$), and (d) fully turbulent flow regime ($Re_p > 300$) [104].

Solid particles in packed bed tanks act as natural distributors, and the impact of flow velocity on the thermal performance of packed bed tanks is smaller than that on SMTHS tanks. For packed bed tanks in laminar flow conditions, the effect of inlet velocity on thermal performance is minimal. However, as turbulence develops, an increase in Reynolds number and flow rate leads to a decrease in heat transfer and storage efficiency [104]. The authors of Ref. [27] reported that for packed bed THS tanks, the efficiency first increases and then decreases as the flow rate increases. Both total discharging and charging times decrease with increasing inlet salt velocity, and for the discharging process, the outlet temperatures are almost the same at different flow velocities [20].

For structured THS tanks, an increase in flow velocity results in reduced discharging efficiency for systems with different solid TESM structures. In the case of channel-embedded structures, the effective discharging efficiency significantly decreases from 83.1% to 60% when the fluid inlet velocity increases from 0.002 m/s to 0.01 m/s, while the efficiency drop in packed bed structures is negligible [50]. An increase in flow velocity also causes an increase in pressure drop in structured THS systems. As the HTF inlet velocity increases from 0.01 m/s to 0.1 m/s, the pump power consumption increases by more than 24 times [137]. In cascaded THS tanks, an increase in flow velocity results in decreased charging time and exergy efficiency [129]. In hybrid sensible–latent THS tanks, an increase in flow velocity can enhance the heat transfer rate, improving charging and discharging efficiency but reducing effective discharging time [57].

For indirect THS tanks, the outlet temperature of the coil, stored thermal energy, and extent of thermal stratification decrease with an increase in coil flow rate, while the discharging rate and discharging efficiency increase. An increase in charging flow rate results in an increase in the rate of thermal energy input to the tank, average heat extraction rate, and cumulative energy discharged, while coil outlet temperature, discharging efficiency, and operational duration decrease with the thermal stratification degradation [140].

In conclusion, an increase in flow velocity enhances heat transfer rates but also results in greater fluid disturbance and pressure drop. Simultaneously, increased flow velocity reduces charging time, minimizing heat losses to the surroundings [137]. Considering tank wall heat losses, an optimal flow velocity can be determined [141].

5.2.2. Temperature

For THS systems, especially sensible heat THS systems, the temperature plays a crucial role in determining the storage capacity. The higher the temperature of the

high-temperature HTF entering the THS tank, the more heat can be stored in the high-temperature zone of the tank. Additionally, the charging and discharging of the tank can be controlled by adjusting the cut-off temperature (also called stop temperature), which is the outlet temperature of the tank.

When the cut-off threshold (also called stop threshold) is denoted as κ, the outlet cut-off temperature during charging is defined as follows:

$$T_{out}^{ch} = T_L + \kappa_{ch} \cdot (T_H - T_L) \tag{33}$$

Among them, T_H is the temperature of the high-temperature fluid injected during charging, and T_L is the temperature of the low-temperature fluid injected during discharge. Similarly, the outlet cut-off temperature during discharge can be defined as follows:

$$T_{out}^{d} = T_L - \kappa_{d} \cdot (T_H - T_L) \tag{34}$$

During charging, the charging process is halted when the outlet temperature exceeds the cut-off temperature, and during discharging, the discharge process is halted when the outlet temperature falls below the cut-off temperature.

The cut-off temperature has an impact on the efficiency of the THS tank. Numerical research by Vannerem et al. indicates that the utilization rate decreases with a strict threshold ($\kappa_{ch} = \kappa_d = 0.05$), and at hybrid thresholds (strict during charge, soft during discharge), exergy efficiency increases overall [29]. For a THS system with a constant inlet flow rate, temperature thresholds can be used to set the duration of charging and discharging.

Higher inlet temperatures during charging can reduce charging time [137,140]. Inlet temperature also affects the efficiency of the THS tank. For SMTHS tanks, larger temperature differentials favor thermal stratification during charging, with less noticeable effects during discharging [46]. After optimizing the distributor for SMTHS tanks, the impact of temperature differentials on tank performance appears to be negligible [109]. Increasing the inlet temperature or decreasing the outlet temperature can help the THS tank maintain higher efficient discharge capability under high flow rates, which is crucial for improving charging and discharging power [16].

For DMTHS tanks, Xie et al. found that as the maximum operating temperature of the tank increases, charging efficiency slightly decreases due to increased heat losses, while the overall efficiency slightly increases [15]. Numerical simulation results by Nandi et al. indicate that the inlet fluid temperature has no significant impact on storage efficiency [104]. During discharging, the thickness of the thermocline zone decreases with the increase in the temperature of the cold HTF, and after a prolonged discharging process, the thickness shows less variation with the temperature of the cold HTF [20]. An increased temperature difference between the hot and cold fluids in the tank leads to higher axial maximum mechanical stresses, while an increase in ambient temperature slightly reduces the normalized stress on the tank wall [20]. An increase in the initial temperature of the tank reduces its heat storage capacity [103].

In practical operations, inlet and outlet temperatures are often determined by the heat source and heat consumers. Auxiliary heat exchangers can be used to adjust inlet and outlet temperatures, but this may introduce additional costs and efficiency losses, necessitating further research.

5.2.3. Charging and Discharging Strategies

In this section, different charging and discharging strategies in recent studies are discussed in a categorized manner, and their highlights are summarized in Table 5.

Table 5. Charging and discharging strategies and their highlights.

Reference	Strategy	Type	Approach	Characteristics
[65]	Dynamic dual mode	SMTHS	Ex	Describe the thermal stratification phenomenon of THS storage tanks used for cooking under three different SCAD modes.
[126]	Dynamic dual mode	Indirect SMTHS	Ex/Nu	The initial thermocline zone split into primary and secondary thermocline zones, which expand with time and increasing coil flow rate.
[9]	Dynamic dual mode	DMTHS	Ex	The increase in discharge flow increases the overall charge–discharge time, thickening the thermocline, and there exists a "perfect flow" that maximizes discharge efficiency and utilization rate.
[84]	Standby mode, reverse charging method, and forward charging method	DMTHS	Ex	In long standby mode, reverse charging has twice the exergy loss of forward charging, with significantly lower energy and exergy efficiency than forward charging.
[129]	Series charging and discharging method, parallel charging and discharging method, and series charging combined with parallel discharging method	Multi-tank indirect SMTHS	Ex/Nu	The parallel charging and discharging method has lower discharge temperatures, and the series–parallel combination method results in unequal discharge temperatures of the three tanks, with the series charging and discharging method being the best strategy.
[130]	Series charging method	Multi-tank SMTHS	Nu	The thermocline zone can move between multiple tanks connected in series, and the multi-tank THS reduces thermocline energy loss.
[131]	Segmented charging method	Segmented bed	Nu	Segmented charging can control the movement of thermal fronts and maintain thermal stratification, and the segmented position has a slight impact on the maximum energy storage capacity of the system.
[105,132]	Segmented charging and discharging method	Segmented bed	Nu	Segmentation reduces conduction losses during the charging mode, and segmented THS tanks have better performance and economics than radial flow THS tanks and axial flow THS tanks.
[30]	Two cycle control scenarios: time-based and temperature-based	Layered bed	Ex	Layering reduces pressure loss by about 64% while producing a narrower thermocline. In the time-based scenario, the layered and simple modes have comparable thermal performance, with lower exit loss in the layered mode. In the temperature-based scenario, the layered mode reaches the steady state earlier and has better performance.
[118]	Full charge–partial discharge scheme, partial charge–partial discharge scheme	Combined sensible–latent THS, cascaded THS	Nu	The overall efficiency of the full charge–partial discharge scheme is much higher than the partial charge–partial discharge scheme.
[133]	Seven charging and discharging strategies consisting of four charging strategies and five discharging strategies	Two-tank TES, indirect two-tank TES, DMTHS, indirect DMTHS	Nu	The annual electricity production of a solar thermal power plant with a THS system is always lower than that of the same plant with a two-tank system. The electricity yield and fossil fuel consumption for the seven strategies analyzed show similar behavior in direct and indirect configurations. The optimal strategy for the charging process is to partially extract the thermocline region to feed the solar field to the maximum allowable inlet temperature. The best strategies for discharge technology are to completely extract the thermocline region, and the feeding sequence to various components of the power plant varies according to the annual power generation or annual fossil fuel consumption.

In the Approach column, Ex represents experimental studies, and Nu represents numerical studies.

According to the charging and discharging status of the THS system, there are three strategies: dynamic single mode, dynamic dual mode, and static mode [142]. In the dynamic single mode, either charging or discharging is conducted independently. Dynamic dual mode, also known as simultaneous charging and discharging (SCAD) mode, involves the simultaneous charging and discharging of the THS tank. The static mode refers to the tank being in an isolated state, with no inflow or outflow of the HTF. Mawire et al. conducted experimental research on the SCAD mode of THS tanks, testing three SCAD mode experimental cases and describing the thermal stratification phenomenon and charging power of the tank [83]. Khurana's research group experimentally and numerically studied the SCAD mode of a thermocline water tank equipped with a spiral discharge coil [140]. In the dynamic dual mode, the initial thermocline zone split into primary and secondary thermocline zones as it descended through the spiral discharge coil, and the thermocline zones expanded with increasing time and coil flow rate. Xi et al. conducted experimental research on the SCAD process of a THS tank filled with PCM capsules, considering three

cases where the charging flow rate remained constant at 0.7 m^3/h, and the discharging flow rates were 0.1 m^3/h, 0.3 m^3/h, and 0.5 m^3/h, respectively [9]. The results showed that an increase in the discharging flow rate would decrease the outlet temperature, increase the thermocline zone thickness, and alter the time of supplying hot water above 69 °C, indicating the existence of a 'perfect flow rate' based on specific discharging requirements.

Depending on the design requirements, some THS tanks need to be charged from the bottom. This reverse charging method concentrates high-temperature fluid at the bottom of the tank, leading to strong natural convection and significant heat exchange, causing an irreversible entropy increase and rapid degradation of the thermocline [98]. Schwarzmayr et al. qualitatively and quantitatively studied the standby efficiency and thermocline degradation of a DMTHS tank, comparing top charging (forward) and bottom charging (reverse) methods [98]. The results indicated that under long standby mode, the exergy losses in reverse charging were twice as much as forward charging, and the energy efficiency (74%) and exergy efficiency (55%) of forward charging were significantly higher than reverse charging (70% and 45%, respectively).

Due to mechanical constraints, a single tank cannot be too high. When the thermal storage capacity demand is large, the THS system will include multiple tanks. Dickinson et al. experimentally and numerically studied the thermal stratification behavior during the charging and discharging processes of three indirect SMTHS tanks in different configurations: series charging and discharging, parallel charging and discharging, and series charging combined with parallel discharging [143]. The results showed that during series charging, the three tanks exhibited sequential stratification, but significant mixing occurred in the latter two tanks. Parallel charging resulted in good stratification in all three tanks, but the overall temperature was lower. The series–parallel combination led to unequal output temperatures in the three tanks. Therefore, series charging and discharging are more practical.

Szczęśniak et al. numerically studied a seasonal THS system for factory air conditioning, simulating multi-tank THS by connecting four thermocline tanks in series, allowing the thermocline zone to move between different tanks [144]. The results indicated that multi-tank THS could reduce thermocline energy losses, but the material required to manufacture four tanks was 80% more than that for a single tank of the same capacity. The schematic of series and parallel charging for the multi-tank THS is shown in Figure 15.
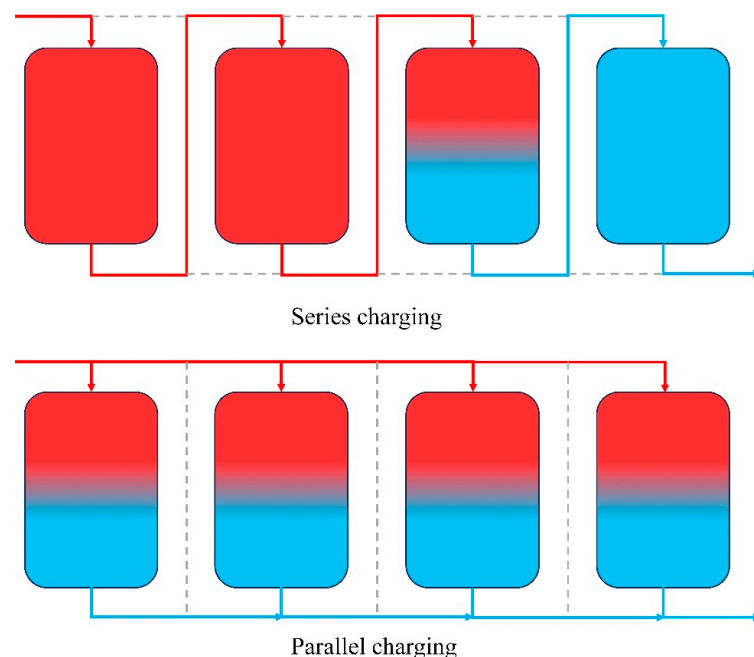

Figure 15. A schematic of series charging and parallel charging for the multi-tank THS.

Crandall and Thacher proposed the concept of segmented beds and conducted numerical studies, dividing the packed bed into three segments and charging each segment from top to bottom to control the movement of the thermal fronts and maintain thermal stratification [145]. Figure 16 shows the charging process of the three-stage segmented THS system. McTigue and White conducted an economic evaluation and thermal–economic optimization of a PTES system with segmented packed beds [146]. The results showed that segmentation could reduce the conduction losses during the storage stage but would increase additional costs (valves and sensors). In the follow-up work, they compared the segmented THS tank with the radial flow THS tank and the axial flow THS tank and found that the segmented storage has the best performance and better economy [120]. However, this analysis did not consider the costs of additional internal structures and control systems, leading to some uncertainties.
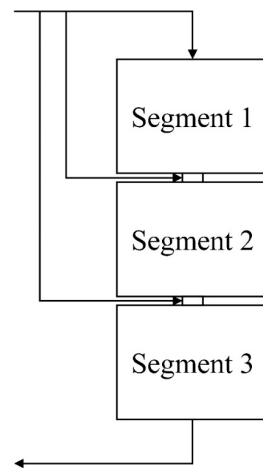

Figure 16. Schematic of segmented THS system.

Ameen et al. experimentally studied a novel layered packed bed THS system, which is part of the world's first grid-scale 150 kWe PTES demonstration system [30]. The layered THS system, controlled by an intelligent Layer Control System, selectively opens or closes gas bypass throttle valves to precisely control the thermal fronts through each layer. Experiments showed that layering could reduce pressure losses by approximately 64%, with minimal changes in round-trip energy efficiency, storage capacity, and utilization rate. Under time-based cycle control, the exit losses from layered THS were reduced. Figure 17 shows different drawing views of the store.

Charging and discharging strategies have a significant impact on the overall efficiency of the THS system, especially when considering continuous cycles. For the system proposed in reference [132], the total efficiency of the fully charged–partially discharged scheme is much higher than that of the partially charged–partially discharged scheme, with a 54.05% increase in efficiency at a charging time of 4 h. Biencinto et al. developed a simulation model using TRNSYS$^©$ 16 software to analyze the annual performance of two-tank or THS systems with synthetic oil (indirect thermal storage) or molten salt (direct thermal storage) as the HTF under different operating strategies [147]. The analysis showed that, in terms of annual electricity generation and fossil fuel consumption, indirect and direct thermal storage exhibited similar trends, and the optimal strategies for both methods might be the same. The best strategy during the charging process was to partially extract the thermocline region, feeding the solar field to its maximum allowable inlet temperature, while the discharging process required a complete extraction of the thermocline region.
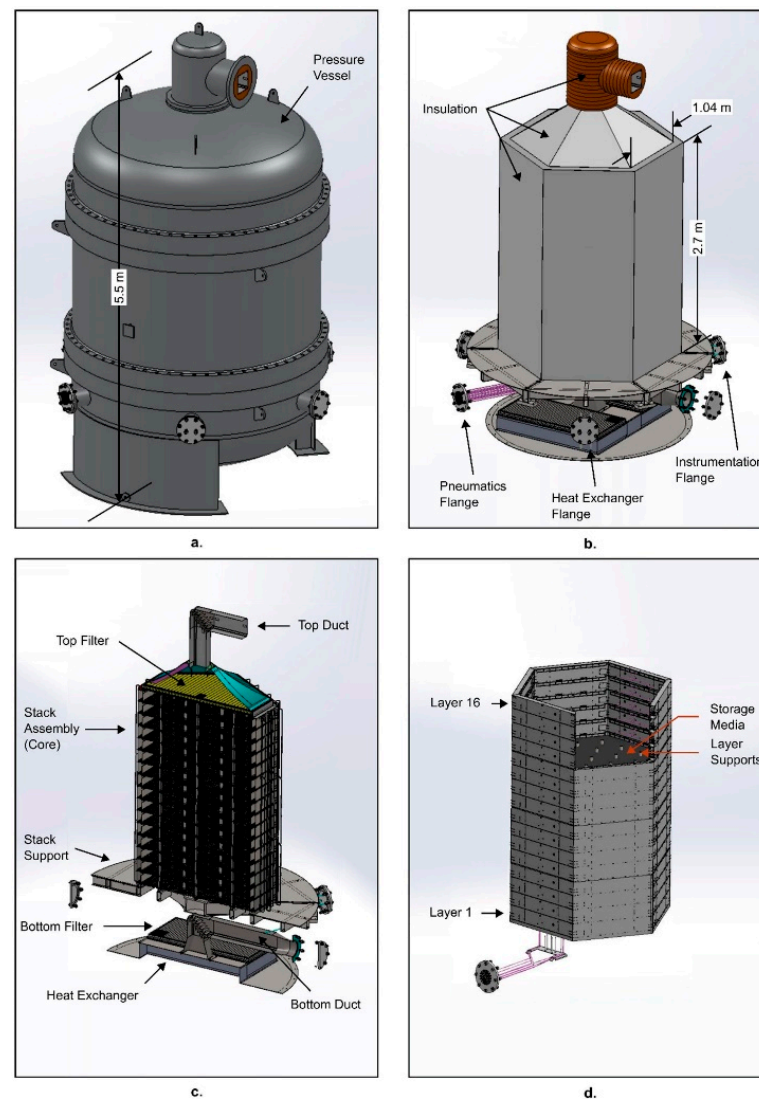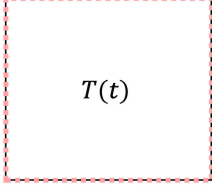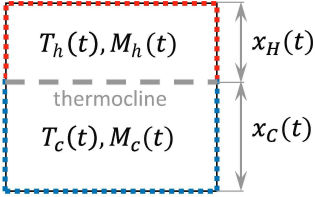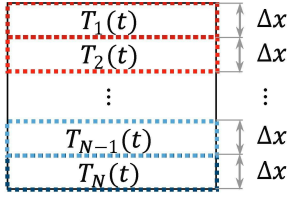
Figure 17. Three-dimensional drawing views of store. (**a**) Complete store, (**b**) without pressure vessel, hard insulation is shown only, (**c**) section through store with complete insulation removed, and (**d**) main core showing stack built up to layer 11 [30].

5.3. Optimization of Thermocline Heat Storage System Numerical Model

Experimental studies on THS systems demand a lot of resources and time, incurring high costs. The technical, economic, and environmental analysis of THS heavily relies on numerical methods due to these challenges. Therefore, the development of fast and accurate models is crucial to expedite research in THS. Various types of models have been developed to investigate different aspects of THS. In the recent literature, software tools employed for numerical studies on THS include Ansys CFX [8], Ansys Fluent [27,46,47], Aspen Hysys [144], COMSOL [79], COMSOL Multiphysics [49,70,127], TRNSYS [42,147], NEST [19], EBSILON [72], and Star-CCM+ [47].

Numerical models can be classified based on their dimensions into 0D, 1D, 2D, and 3D models. While 3D and 2D models vividly depict the flow and heat transfer phenomena within the THS tank, they are computationally expensive and time-consuming. Such models are suitable for analyzing fluid movement in localized areas of the tank, such as inlets, outlets, distributors, and heat exchangers. For large-scale or seasonal system studies, 1D and 0D models are employed to accelerate computational speed. The differences between 0D, quasi-1D, and 1D modeling approaches are shown in Table 6.

Table 6. Differences between 0D, quasi-1-dimensional, and 1D modeling approaches [26].

Approach	Schematic	Principle	Computational Time
0D modeling approach	$T(t)$ $M \cdot c_p \cdot \frac{dT}{dt} = \sum \dot{m} \cdot h + \sum \dot{Q}$	The system is considered as a unique fully mixed region having uniform temperature. The dynamic behavior of the storage is described by the time profile of the uniform temperature inside the tank calculated by solving a single energy balance ordinary differential equation.	5 s
quasi-1D modeling approach	$T_h(t), M_h(t) \quad x_H(t)$ thermocline $T_c(t), M_c(t) \quad x_C(t)$ $\begin{cases} \frac{dM_i}{dt} = \sum \dot{m}_i \\ M_i \cdot c_{p,i} \cdot \frac{dT_i}{dt} = \sum \dot{m}_i \cdot h_i + \sum \dot{Q}_i \end{cases}$ $i = h, c$	The internal volume is subdivided into a hot and a cold region, having uniform temperature and variable boundaries over time. The storage operation is described by the time profiles of the temperatures and masses of the two regions calculated using two energy and mass balance ordinary differential equations.	12 s
1D modeling approach	$T_1(t) \quad \Delta x$ $T_2(t) \quad \Delta x$ $\vdots \quad \vdots$ $T_{N-1}(t) \quad \Delta x$ $T_N(t) \quad \Delta x$ $M_i \cdot c_{p,i} \cdot \frac{dT_i}{dt} = \sum \dot{m}_i \cdot h_i + \sum \dot{Q}_i$ $i = 1, \dots, N$	The tank is discretized into N layers of fixed thickness Δx and uniform temperature, where the layer at the top is defined as layer number 1. The thickness is known by dividing the tank height by the chosen number of layers. N energy balance ordinary differential equations are required to calculate the temperature stratification inside the storage tank as a function of time.	13 s

Palomba and Frazzica provided a comprehensive review of numerical methods used in recent years for THS design and gave simple guidelines for model selection, as shown in Table 7 [148]. However, there is a lack of discussion on 0D models. This section will describe the recent new research on the numerical method for THS optimization.

Table 7. Model selection guidelines [148].

Type of Model	Main Features	Motivation for Choosing the Model
1D	Low computational effort, 2 phases assumed.	Simple geometry of the tank, with no effect of radiant gradient, especially suited for coupling with optimization methods.
2D 1-phase	1 heat equation for both filler and HTF, reduced computational effort.	Systems in which Biot body approximation can be applied. This occurs for small-size filler particles or low Reynolds numbers in the fluid.
2D 2-phase	2 heat equations for filler and HTF.	Suitable for a wide variety of systems, including solid or PCM fillers, vast literature data available, proven reliability and accuracy.
3D	Higher computational effort compared to 1D and 2D cases, higher accuracy.	The evaluation of localized phenomena, the evaluation of complex geometries, i.e., in the distributors.

Szczęśniak et al. established a 3D model to simulate the thermal behavior of a hot water tank and derived a 0D model for temperature stratification based on simulation results [149]. This model accounts for heat loss through the thermocline and can be applied for system-level and seasonal modeling. Raccanello et al. compared the applicability of 0D, quasi-1D, and 1D models for numerical simulations of THS tanks [26]. The 0D

model neglects heat conduction and mass transfer within the tank, while the quasi-1D model disregards energy transfer between different layers within the tank, leading to the underestimation of temperatures during the charging phase and overestimation during the discharging phase. The 1D model can predict performance and thermal stratification with sufficient accuracy.

Odenthal et al. compared four 1D models for packed beds (the Schumann model, the continuous solid-phase model, the single-phase model, and a bidisperse model) under different usage scenarios (single blow operation, cyclic operation, and annual simulations) [48]. The results indicated that for small particles, a single-phase model is suitable, while a bidisperse model is preferable for larger particles. Variable fluid characteristics can be neglected for long-term simulations (cyclic and annual simulations). A 1D model developed by Untrau et al. using a new discretization method, considering Orthogonal Collocation (OC) and Orthogonal Collocation on Finite Elements (OCFE), showed faster solving speed and higher accuracy compared to traditional 1D models [150]. In comparison to multi-node models, the OCFE model used fewer discrete points, resulting in faster computation speed while maintaining the same level of accuracy. The model has been validated with real factory data.

Numerical models predicting the thermal behavior of packed beds can be categorized into continuous methods and discrete methods [151]. Continuous methods are characterized by short computation times and relatively accurate predictions of overall packed bed behavior but are limited in accurately estimating radiation heat transfer [152]. Discrete methods, as documented in the literature, allow for the explicit treatment of radiation through two approaches: short-range [153,154] and long-range [155]. Long-range methods are often based on the Monte Carlo ray tracing (MCRT) method, enabling the calculation of radiation effective thermal conductivity in monodisperse groups of spheres [156]. However, the drawback of this method lies in its high computational cost. Wu et al. proposed an extended thermal discrete element method for calculating conduction–radiation heat transfer in packed beds, with computational costs nearly identical to those required for conduction alone [157]. A new discrete model developed by Cortés et al. integrated a method called Layer View Factor for radiation estimation, demonstrating a significantly lower computation time (9088 times less) compared to the MCRT-KC method [152].

Flueckiger and Garimella developed a model to assess the storage behavior of PCM-filled THS tanks, integrated into a system-level model for CSP plants. This model identified the optimal range of PCM parameters to maximize the annual output of the power plant [128]. Khurana et al. established and validated a 2D axisymmetric numerical model for cylindrical THS tanks [158]. The predictive model, developed using a seven-parameter three-level Box–Behnken Response Surface Methodology, can accurately predict changes in the thermal stratification, entropy production, and storage efficiency of THS tanks.

The performance of the THS system is collectively determined by multiple parameters, and there are interactions among these parameters. It is essential to employ appropriate algorithms to optimize these parameters. Trevisan et al. developed a novel quasi-dynamic boundary evolutionary genetic algorithm for the comprehensive multi-objective optimization of an industrial-scale packed bed THS system, taking into account the levelized cost of storage [159]. Nandi used a CFD–Taguchi combined method to assess the impact of Reynolds number, particle diameter, bed porosity, and tank aspect ratio on the energy storage performance of the tank, determining the optimal conditions and geometric shapes of the system [104]. Le Roux et al. employed a combination of Shannon entropy and a multi-criteria decision-making method using the NSGA-II multi-objective genetic algorithm to optimize the packed bed THS system, considering technical, economic, and environmental aspects [33]. Marti et al. utilized a constrained multi-objective optimization approach to optimize the exergy efficiency and material cost of the packed bed THS system, handling the competing goals of maximizing exergy efficiency and minimizing material costs through Pareto frontiers [103]. Compared to brute-force design methods, the optimization procedure can reduce computation time by 91–99%. Lou et al. introduced a

novel intermediate evaluation metric to characterize the real-time thermal behavior of THS tanks, significantly reducing the computational cost of the optimization problem by at least six times [95].

6. Conclusions and Perspectives

Thermocline heat Storage (THS) is considered a promising solution to address energy challenges and promote sustainable development due to its economic and stable nature. This work reviews the latest research on THS systems, including principles, materials, applications, and optimization methods, and draws the following conclusions:

- SMTHS systems are structurally simple and easy-to-maintain but have lower thermal storage capacity, making them suitable for domestic applications. Distributors are needed to mitigate the impact of the inlet jet on thermal performance.
- DMTHS systems offer large thermal storage capacity and stable performance but require special attention to the thermal ratcheting issue. Strategies such as composite walls, conical storage tanks, and structured tanks can be used to reduce the risk of structural failure. Due to mechanical limitations, the maximum height for packed bed THS systems is 16 m.
- Increasing the aspect ratio can reduce the diffusion of the thermocline zone but may increase heat loss. During long standby modes, spherical and barrel-shaped tanks are the most efficient; parabolic tanks perform better in charge–discharge modes.
- When selecting TESMs, multiple requirements must be considered. Utilizing local natural materials and industrial waste can reduce costs and address waste management issues, but stability and compatibility must be considered.
- The ordered packing of solid TESMs can enhance thermal stratification stability and reduce pressure drop. The cascaded configuration using both sensible and latent heat TESMs can improve the system's thermal performance and efficiency; three–five levels are recommended based on cost and structural considerations.
- Axial downward flow from the top of the tank is the optimal flow direction. For tanks requiring a reverse flow design, distributors should be used to limit the movement of solid particles within the tank to maintain a fixed bed state. Radial flow packed bed structures have low pressure drop and self-insulation properties but lower efficiency.
- Multi-objective optimization is necessary in THS system design. Excessively small particle sizes and high flow rates can significantly reduce THS system performance, and insulation treatment is crucial in any design.
- For multi-tank THS systems, a series configuration is recommended to achieve stable outlet temperatures and reduce the diffusion of thermal gradients.
- Charging and discharging strategies significantly affect the overall efficiency of THS, especially for continuous cyclic operation. Numerical studies of large-scale or seasonal systems require one-dimensional models to accelerate computation speed.
- THS has bright application prospects in fields such as hydrogen storage and waste heat recovery, with both environmental and economic benefits.

In light of the deficiencies in current research, we propose the following recommendations and perspectives:

- The arrangement of solid TESMs in structured THS tanks needs to be optimized to improve heat transfer efficiency and thermal efficiency.
- There is a lack of experimental research to verify the effectiveness and feasibility for orderly bed-type THS tanks.
- Research on the thermal cycling and long-term operation of THS systems is scarce, and attention should be paid to the cycling efficiency and long-term performance of THS heating systems under different operating strategies.
- Further in-depth research on the thermal ratcheting issue of packed bed THS systems is needed to determine the specific conditions that may lead to structural damage.

Data Availability Statement: Data is contained within the article.

Conflicts of Interest: The authors declare no conflict of interest.

References

1. Brockway, P.E.; Owen, A.; Brand-Correa, L.I.; Hardt, L. Estimation of global final-stage energy-return-on-investment for fossil fuels with comparison to renewable energy sources. *Nat. Energy* **2019**, *4*, 612–621. [CrossRef]
2. Manowska, A.; Nowrot, A. The Importance of Heat Emission Caused by Global Energy Production in Terms of Climate Impact. *Energies* **2019**, *12*, 3069. [CrossRef]
3. Koohi-Fayegh, S.; Rosen, M.A. A review of energy storage types, applications and recent developments. *J. Energy Storage* **2020**, *27*, 101047. [CrossRef]
4. Suresh, C.; Saini, R.P. Thermal performance of sensible and latent heat thermal energy storage systems. *Int. J. Energy Res.* **2020**, *44*, 4743–4758. [CrossRef]
5. Pizzolato, A.; Donato, F.; Verda, V.; Santarelli, M.; Sciacovelli, A. CSP plants with thermocline thermal energy storage and integrated steam generator–Techno-economic modeling and design optimization. *Energy* **2017**, *139*, 231–246. [CrossRef]
6. Angelini, G.; Lucchini, A.; Manzolini, G. Comparison of Thermocline Molten Salt Storage Performances to Commercial Two-tank Configuration. *Energy Procedia* **2014**, *49*, 694–704. [CrossRef]
7. Cascetta, M.; Petrollese, M.; Oyekale, J.; Cau, G. Thermocline vs. two-tank direct thermal storage system for concentrating solar power plants: A comparative techno-economic assessment. *Int. J. Energy Res.* **2021**, *45*, 17721–17737. [CrossRef]
8. Alesbe, I.; Abdul Wahhab, H.A.; Aljabair, S. Transient study of thermal stratification of full-scale chilled water storage tank during optimum discharge condition. *J. Energy Storage* **2023**, *65*, 107236. [CrossRef]
9. Xi, X.; Zhang, Z.; Wei, H.; Chen, Z.; Du, X. Experimental Study of Simultaneous Charging and Discharging Process in Thermocline Phase Change Heat Storage System Based on Solar Energy. *Sustainability* **2023**, *15*, 7322. [CrossRef]
10. Armfield, S.W.; Kirkpatrick, M.P.; Milton-McGurk, L.; Williamson, N. Characterising entrainment in fountains and negatively buoyant jets. *J. Fluid Mech.* **2022**, *939*, A29. [CrossRef]
11. Advaith, S.; Parida, D.R.; Aswathi, K.T.; Dani, N.; Chetia, U.K.; Chattopadhyay, K.; Basu, S. Experimental investigation on single-medium stratified thermal energy storage system. *Renew. Energy* **2021**, *164*, 146–155. [CrossRef]
12. Zachár, A. Analytic solution for convection dominant heat transport induced by buoyant jet entrainment inside hot fluid storage tanks. *Sol. Energy* **2020**, *195*, 239–248. [CrossRef]
13. Yi, Y.; Nakayama, A. An analytical study on transient thermal behavior of a packed-bed molten salt thermocline thermal storage. *Int. J. Heat Mass Transf.* **2023**, *209*, 124095. [CrossRef]
14. Li, M.-J.; Qiu, Y.; Li, M.-J. Cyclic thermal performance analysis of a traditional Single-Layered and of a novel Multi-Layered Packed-Bed molten salt Thermocline Tank. *Renew. Energy* **2018**, *118*, 565–578. [CrossRef]
15. Xie, B.; Baudin, N.; Soto, J.; Fan, Y.; Luo, L. Experimental and numerical study on the thermocline behavior of packed-bed storage tank with sensible fillers. *Renew. Energy* **2023**, *209*, 106–121. [CrossRef]
16. He, Z.; Qian, Y.; Xu, C.; Yang, L.; Du, X. Static and dynamic thermocline evolution in the water thermocline storage tank. *Energy Procedia* **2019**, *158*, 4471–4476. [CrossRef]
17. Flueckiger, S.; Yang, Z.; Garimella, S.V. An integrated thermal and mechanical investigation of molten-salt thermocline energy storage. *Appl. Energy* **2011**, *88*, 2098–2105. [CrossRef]
18. Elfeky, K.E.; Mohammed, A.G.; Ahmed, N.; Wang, Q. Thermo-mechanical investigation of the multi-layer thermocline tank for parabolic trough power plants. *Energy* **2023**, *268*, 126749. [CrossRef]
19. González, I.; Pérez-Segarra, C.D.; Lehmkuhl, O.; Torras, S.; Oliva, A. Thermo-mechanical parametric analysis of packed-bed thermocline energy storage tanks. *Appl. Energy* **2016**, *179*, 1106–1122. [CrossRef]
20. Wang, G.; Yu, S.; Niu, S.; Chen, Z.; Hu, P. A comprehensive parametric study on integrated thermal and mechanical performances of molten-salt-based thermocline tank. *Appl. Therm. Eng.* **2020**, *170*, 115010. [CrossRef]
21. Motte, F.; Bugler-Lamb, S.L.; Falcoz, Q.; Py, X. Numerical Study of a Structured Thermocline Storage Tank Using Vitrified Waste as Filler Material. *Energy Procedia* **2014**, *49*, 935–944. [CrossRef]
22. Mawire, A.; Taole, S.H. A comparison of experimental thermal stratification parameters for an oil/pebble-bed thermal energy storage (TES) system during charging. *Appl. Energy* **2011**, *88*, 4766–4778. [CrossRef]
23. Castell, A.; Medrano, M.; Solé, C.; Cabeza, L.F. Dimensionless numbers used to characterize stratification in water tanks for discharging at low flow rates. *Renew. Energy* **2010**, *35*, 2192–2199. [CrossRef]
24. Pradeep, N.; Reddy, K.S. Performance enhancement of packed bed thermal energy storage system for solar cogeneration of power and potable water production. *J. Clean. Prod.* **2023**, *404*, 136754. [CrossRef]
25. Rendall, J.; Abu-Heiba, A.; Gluesenkamp, K.; Nawaz, K.; Worek, W.; Elatar, A. Nondimensional convection numbers modeling thermally stratified storage tanks: Richardson's number and hot-water tanks. *Renew. Sustain. Energy Rev.* **2021**, *150*, 111471. [CrossRef]

26. Raccanello, J.; Rech, S.; Lazzaretto, A. Simplified dynamic modeling of single-tank thermal energy storage systems. *Energy* **2019**, *182*, 1154–1172. [CrossRef]

27. Ortega-Fernández, I.; Loroño, I.; Faik, A.; Uriz, I.; Rodríguez-Aseguinolaza, J.; D'Aguanno, B. Parametric analysis of a packed bed thermal energy storage system. *AIP Conf. Proc.* **2017**, *1850*, 080021. [CrossRef]

28. Haller, M.Y.; Cruickshank, C.A.; Streicher, W.; Harrison, S.J.; Andersen, E.; Furbo, S. Methods to determine stratification efficiency of thermal energy storage processes–Review and theoretical comparison. *Sol. Energy* **2009**, *83*, 1847–1860. [CrossRef]

29. Vannerem, S.; Neveu, P.; Falcoz, Q. Thermal cycle performance of thermocline storage: Numerical and experimental exergy analysis. *Energy* **2023**, *278*, 127647. [CrossRef]

30. Ameen, M.T.; Ma, Z.; Smallbone, A.; Norman, R.; Roskilly, A.P. Experimental study and analysis of a novel layered packed-bed for thermal energy storage applications: A proof of concept. *Energy Convers. Manag.* **2023**, *277*, 116648. [CrossRef]

31. Cárdenas, B.; Davenne, T.R.; Wang, J.; Ding, Y.; Jin, Y.; Chen, H.; Wu, Y.; Garvey, S.D. Techno-economic optimization of a packed-bed for utility-scale energy storage. *Appl. Therm. Eng.* **2019**, *153*, 206–220. [CrossRef]

32. Ingenhoven, P.; Lee, L.; Saw, W.; Rafique, M.M.; Potter, D.; Nathan, G.J. Techno-economic assessment from a transient simulation of a concentrated solar thermal plant to deliver high-temperature industrial process heat. *Renew. Sustain. Energy Rev.* **2023**, *185*, 113626. [CrossRef]

33. Le Roux, D.; Olivès, R.; Neveu, P. Combining entropy weight and TOPSIS method for selection of tank geometry and filler material of a packed-bed thermal energy storage system. *J. Clean. Prod.* **2023**, *414*, 137588. [CrossRef]

34. Ingenhoven, P.; Saw, W.; Chinnici, A.; Potter, D.; Nathan, G.; Rafique, M.M.; Lee, K.L.; Jafarian, M. Energetic Assessment of a High Temperature Packed Bed Storage System in Combination with a Solar Expanding-Vortex Particle Receiver. In Proceedings of the ISES Solar World Congress 2021, Online, 25–29 October 2021; pp. 1–10.

35. Singh, P.L.; Deshpandey, S.D.; Jena, P.C. Thermal performance of packed bed heat storage system for solar air heaters. *Energy Sustain. Dev.* **2015**, *29*, 112–117. [CrossRef]

36. Andharia, J.K.; Markam, B.; Dzhonova, D.; Maiti, S. A comparative performance analysis of sensible and latent heat based storage in a small-scale solar thermal dryer. *J. Energy Storage* **2022**, *45*, 103764. [CrossRef]

37. Cascetta, M.; Licheri, F.; Merchán, R.P.; Petrollese, M. Operating performance of a Joule-Brayton pumped thermal energy storage system integrated with a concentrated solar power plant. *J. Energy Storage* **2023**, *73*, 108865. [CrossRef]

38. Junli, C.; Yanping, Z.; Chongzhe, Z.; Yulong, X.; Yuming, O. Thermal performance analysis of a thermocline storage tank with integrated annular distributors. *Front. Energy Res.* **2023**, *11*. [CrossRef]

39. Wang, G.; Xie, Z.; Wang, B.; Lin, J. Comparison study on operation and mechanical characteristics of liquid sodium thermoclinic heat storage tank using different solid filling materials. *Case Stud. Therm. Eng.* **2023**, *49*, 103415. [CrossRef]

40. Aggarwal, A.; Goyal, N.; Kumar, A. Thermal characteristics of sensible heat storage materials applicable for concentrated solar power systems. *Mater. Today Proc.* **2021**, *47*, 5812–5817. [CrossRef]

41. Ding, Z.; Wu, W.; Leung, M. Advanced/hybrid thermal energy storage technology: Material, cycle, system and perspective. *Renew. Sustain. Energy Rev.* **2021**, *145*, 111088. [CrossRef]

42. Zhou, C.; Wang, Y.; Li, J.; Ma, X.; Li, Q.; Yang, M.; Zhao, X.; Zhu, Y. Simulation and economic analysis of an innovative indoor solar cooking system with energy storage. *Sol. Energy* **2023**, *263*, 111816. [CrossRef]

43. Ushak, S.; Fernández, A.G.; Prieto, C.; Grageda, M. 3-Advances in molten salt storage systems using other liquid sensible storage media for heat storage. In *Advances in Thermal Energy Storage Systems*, 2nd ed.; Cabeza, L.F., Ed.; Woodhead Publishing: Duxford, UK, 2021; pp. 55–81.

44. Abedigamba, O.P.; Mndeme, F.S.; Mawire, A.; Bahadur, I. Thermo-physical properties and thermal energy storage performance of two vegetable oils. *J. Energy Storage* **2023**, *61*, 106774. [CrossRef]

45. Chekifi, T.; Boukraa, M. Thermocline storage for concentrated solar power plants: Descriptive review and critical analysis. *J. Energy Storage* **2022**, *55*, 105773. [CrossRef]

46. Lou, W.; Xie, B.; Aubril, J.; Fan, Y.; Luo, L.; Arrivé, A. Optimized flow distributor for stabilized thermal stratification in a single-medium thermocline storage tank: A numerical and experimental study. *Energy* **2023**, *263*, 125709. [CrossRef]

47. Cagnoli, M.; Gaggioli, W.; Liberatore, R.; Russo, V.; Zanino, R. CFD modelling of an indirect thermocline energy storage prototype for CSP applications. *Sol. Energy* **2023**, *259*, 86–98. [CrossRef]

48. Odenthal, C.; Tombrink, J.; Klasing, F.; Bauer, T. Comparative study of models for packed bed molten salt storage systems. *Appl. Therm. Eng.* **2023**, *226*, 120245. [CrossRef]

49. Al-Azawii, M.M.S.; Alhamdi, S.F.H.; Braun, S.; Hoffmann, J.-F.; Calvet, N.; Anderson, R. Thermocline in packed bed thermal energy storage during charge-discharge cycle using recycled ceramic materials-Commercial scale designs at high temperature. *J. Energy Storage* **2023**, *64*, 107209. [CrossRef]

50. Wu, M.; Li, M.; Xu, C.; He, Y.; Tao, W. The impact of concrete structure on the thermal performance of the dual-media thermocline thermal storage tank using concrete as the solid medium. *Appl. Energy* **2014**, *113*, 1363–1371. [CrossRef]

51. Grirate, H.; Agalit, H.; Zari, N.; Elmchaouri, A.; Molina, S.; Couturier, R. Experimental and numerical investigation of potential filler materials for thermal oil thermocline storage. *Sol. Energy* **2016**, *131*, 260–274. [CrossRef]

52. Elouali, A.; Kousksou, T.; El Rhafiki, T.; Hamdaoui, S.; Mahdaoui, M.; Allouhi, A.; Zeraouli, Y. Physical models for packed bed: Sensible heat storage systems. *J. Energy Storage* **2019**, *23*, 69–78. [CrossRef]

53. Elfeky, K.E.; Mohammed, A.G.; Wang, Q. Thermo-economic evaluation of PCM layer thickness change on the performance of the hybrid heat storage tank for concentrating solar power plants. *Energy* **2022**, *253*, 124128. [CrossRef]
54. Wang, F.; Zhang, C.; Liu, J.; Fang, X.; Zhang, Z. Highly stable graphite nanoparticle-dispersed phase change emulsions with little supercooling and high thermal conductivity for cold energy storage. *Appl. Energy* **2017**, *188*, 97–106. [CrossRef]
55. Huang, X.; Lin, Y.; Alva, G.; Fang, G. Thermal properties and thermal conductivity enhancement of composite phase change materials using myristyl alcohol/metal foam for solar thermal storage. *Sol. Energy Mater. Sol. Cells* **2017**, *170*, 68–76. [CrossRef]
56. Rostami, S.; Afrand, M.; Shahsavar, A.; Sheikholeslami, M.; Kalbasi, R.; Aghakhani, S.; Shadloo, M.S.; Oztop, H.F. A review of melting and freezing processes of PCM/nano-PCM and their application in energy storage. *Energy* **2020**, *211*, 118698. [CrossRef]
57. Zahid, M.S.; Ahmed, N.; Qaisrani, M.A.; Mahmood, M.; Ali, M.; Waqas, A.; Assadi, M. Charging and discharging characterization of a novel combined sensible-latent heat thermal energy storage system by experimental investigations for medium temperature applications. *J. Energy Storage* **2022**, *55*, 105612. [CrossRef]
58. Ali, H.M.; Rehman, T.-u.; Arıcı, M.; Said, Z.; Duraković, B.; Mohammed, H.I.; Kumar, R.; Rathod, M.K.; Buyukdagli, O.; Teggar, M. Advances in thermal energy storage: Fundamentals and applications. *Prog. Energy Combust. Sci.* **2024**, *100*, 101109. [CrossRef]
59. Chen, J.; Feng, B.; Wang, W.; Liang, Y.; Zhang, W.; Li, X.; Li, C.; Wang, N.; Shi, Z. Cobalt nanoparticles supported on nitrogen-doped carbon nanotubes for the efficient oxygen reduction reaction in Mg-air battery. *J. Alloys Compd.* **2024**, *983*, 173878. [CrossRef]
60. Molina, S.; Haillot, D.; Deydier, A.; Bedecarrats, J.-P. Material screening and compatibility for thermocline storage systems using thermal oil. *Appl. Therm. Eng.* **2019**, *146*, 252–259. [CrossRef]
61. Mahammod, B.P.; Barua, E.; Deb, P.; Deoghare, A.B.; Pandey, K.M. Investigation of Physico-mechanical Behavior, Permeability and Wall Shear Stress of Porous HA/PMMA Composite Bone Scaffold. *Arab. J. Sci. Eng.* **2020**, *45*, 5505–5515. [CrossRef]
62. Yu, S.; Han, D.; He, W.; Zhou, M.; Zhu, L.; Gao, Y.; Cui, G.; Peng, T. Analysis and optimization of transient heat dissipation characteristics of high power resistors with a sensible heat storage method. *Appl. Therm. Eng.* **2023**, *226*, 120246. [CrossRef]
63. Tiskatine, R.; Aharoune, A.; Bouirden, L.; Ihlal, A. Identification of suitable storage materials for solar thermal power plant using selection methodology. *Appl. Therm. Eng.* **2017**, *117*, 591–608. [CrossRef]
64. Amiri, L.; Ermagan, H.; Kurnia, J.C.; Hassani, F.; Sasmito, A.P. Progress on rock thermal energy storage (RTES): A state of the art review. *Energy Sci. Eng.* **2024**, *12*, 410–437. [CrossRef]
65. Jemmal, Y.; Zari, N.; Maaroufi, M. Thermophysical and chemical analysis of gneiss rock as low cost candidate material for thermal energy storage in concentrated solar power plants. *Sol. Energy Mater. Sol. Cells* **2016**, *157*, 377–382. [CrossRef]
66. El Alami, K.; Asbik, M.; Agalit, H. Identification of natural rocks as storage materials in thermal energy storage (TES) system of concentrated solar power (CSP) plants—A review. *Sol. Energy Mater. Sol. Cells* **2020**, *217*, 110599. [CrossRef]
67. Katekar, V.P.; Rao, A.B.; Sardeshpande, V.R. An experimental investigation to optimise pebbles-based sensible heat storage system: An exploration to improve thermal efficiency of solar devices. *J. Energy Storage* **2023**, *73*, 108964. [CrossRef]
68. Wang, J.; Huang, Y. Exploration of steel slag for thermal energy storage and enhancement by Na_2CO_3 modification. *J. Clean. Prod.* **2023**, *395*, 136289. [CrossRef]
69. Yang, X.; Cai, Z. An analysis of a packed bed thermal energy storage system using sensible heat and phase change materials. *Int. J. Heat Mass Transf.* **2019**, *144*, 118651. [CrossRef]
70. Canneto, G.; Tizzoni, A.C.; Sau, S.; Mansi, E.; Gaggioli, W.; Spadoni, A.; Corsaro, N.; Capocelli, M.; Caputo, G.; Galindo, F.; et al. Thermocline Thermal Storage for Concentrated Solar Power Applications: Characterization of Novel Nitrate Salt Mixtures. *J. Sol. Energy Eng.* **2023**, *145*, 031001. [CrossRef]
71. Lucio-Martin, T.; Martin, M.; Guerreiro, L.; Villardón, R.S.; Lopez, J.; Alonso, M.C. Thermal performance of a hybrid steel-concrete tank section for thermal energy storage in concentrated solar power plants. *J. Energy Storage* **2023**, *60*, 106630. [CrossRef]
72. El Kouihen, F.; Filali Baba, Y.; AitOusaleh, H.; Elharrak, A.; Elalami, K.; Bennouna, E.; Faik, A. Investigation of thermal energy storage system based on mining by-products for the recovery of Moroccan mining industrial waste heat. *Appl. Therm. Eng.* **2023**, *230*, 120708. [CrossRef]
73. Al-Azawii, M.M.S.; Alhamdi, S.F.H.; Braun, S.; Hoffmann, J.-F.; Calvet, N.; Anderson, R. Experimental study on packed-bed thermal energy storage using recycled ceramic as filler materials. *J. Energy Storage* **2021**, *44*, 103375. [CrossRef]
74. Hong, D.; Yin, Z.; Yan, S.; Xu, W. Fine grained Al_2O_3/SiC composite ceramic tool material prepared by two-step microwave sintering. *Ceram. Int.* **2019**, *45*, 11826–11832. [CrossRef]
75. Wu, Y.-T.; Li, Y.; Ren, N.; Zhi, R.-P.; Ma, C.-F. Experimental study on the thermal stability of a new molten salt with low melting point for thermal energy storage applications. *Sol. Energy Mater. Sol. Cells* **2018**, *176*, 181–189. [CrossRef]
76. Li, Q.; Cong, L.; Zhang, X.; Dong, B.; Zou, B.; Du, Z.; Xiong, Y.; Li, C. Fabrication and thermal properties investigation of aluminium based composite phase change material for medium and high temperature thermal energy storage. *Sol. Energy Mater. Sol. Cells* **2020**, *211*, 110511. [CrossRef]
77. Fernández, Á.G.; Pineda, F.; Fuentealba, E.; Jullian, D.; Mallco, A.; Walczak, M. Compatibility of alumina forming alloys with LiNO3-containing molten salts for solar thermal plants. *J. Energy Storage* **2022**, *48*, 103988. [CrossRef]
78. Lincu, D.; Ioniţă, S.; Mocioiu, O.C.; Berger, D.; Matei, C.; Mitran, R.A. Aluminum doping of mesoporous silica as a promising strategy for increasing the energy storage of shape stabilized phase change materials containing molten $NaNO_3$: KNO_3 eutectic mixture. *J. Energy Storage* **2022**, *49*, 104188. [CrossRef]

79. Nualsing, D.; Pannucharoenwong, N.; Echaroj, S.; Rattanadecho, P. Investigation of molten salts incorporated with anodic aluminum oxide as thermal energy storage fluid on heat transfer efficiency. *Case Stud. Therm. Eng.* **2023**, *49*, 103258. [CrossRef]
80. Wang, G.; Wang, T.; Han, W. Cyclic and standby behavior evaluations of liquid lead-bismuth eutectic thermal energy storage tank for concentrated solar power. *Case Stud. Therm. Eng.* **2022**, *29*, 101729. [CrossRef]
81. Suresh, C.; Saini, R.P. An experimental study on the performance evaluation of a combined sensible-latent heat thermal energy storage. *Int. J. Energy Res.* **2021**, *45*, 5730–5746. [CrossRef]
82. Spur, R.; Fiala, D.; Nevrala, D.; Probert, D. Performances of modern domestic hot-water stores. *Appl. Energy* **2006**, *83*, 893–910. [CrossRef]
83. Mawire, A.; Taole, S.H.; Van den Heetkamp, R.R.J. Experimental investigation on simultaneous charging and discharging of an oil storage tank. *Energy Convers. Manag.* **2013**, *65*, 245–254. [CrossRef]
84. He, W.; Wang, J.; Wang, Y.; Ding, Y.; Chen, H.; Wu, Y.; Garvey, S. Study of cycle-to-cycle dynamic characteristics of adiabatic Compressed Air Energy Storage using packed bed Thermal Energy Storage. *Energy* **2017**, *141*, 2120–2134. [CrossRef]
85. Peng, H.; Shan, X.; Yang, Y.; Ling, X. A study on performance of a liquid air energy storage system with packed bed units. *Appl. Energy* **2018**, *211*, 126–135. [CrossRef]
86. Wang, L.; Lin, X.; Chai, L.; Peng, L.; Yu, D.; Liu, J.; Chen, H. Unbalanced mass flow rate of packed bed thermal energy storage and its influence on the Joule-Brayton based Pumped Thermal Electricity Storage. *Energy Convers. Manag.* **2019**, *185*, 593–602. [CrossRef]
87. Daschner, R.; Binder, S.; Mocker, M. Pebble bed regenerator and storage system for high temperature use. *Appl. Energy* **2013**, *109*, 394–401. [CrossRef]
88. Schwarzmayr, P.; Birkelbach, F.; Walter, H.; Javernik, F.; Schwaiger, M.; Hofmann, R. Packed bed thermal energy storage for waste heat recovery in the iron and steel industry: A cold model study on powder hold-up and pressure drop. *J. Energy Storage* **2024**, *75*, 109735. [CrossRef]
89. Li, G.; Zheng, X. Thermal energy storage system integration forms for a sustainable future. *Renew. Sustain. Energy Rev.* **2016**, *62*, 736–757. [CrossRef]
90. Petrollese, M.; Cascetta, M.; Tola, V.; Cocco, D.; Cau, G. Pumped thermal energy storage systems integrated with a concentrating solar power section: Conceptual design and performance evaluation. *Energy* **2022**, *247*, 123516. [CrossRef]
91. Chandra, Y.P.; Matuska, T. Stratification analysis of domestic hot water storage tanks: A comprehensive review. *Energy Build.* **2019**, *187*, 110–131. [CrossRef]
92. Gaggioli, W.; Fabrizi, F.; Tarquini, P.; Rinaldi, L. Experimental Validation of the Innovative Thermal Energy Storage Based on an Integrated System "Storage Tank/Steam Generator". *Energy Procedia* **2015**, *69*, 822–831. [CrossRef]
93. Tiwari, S.; Sharma, P. Integration of metal hydride reactor with thermocline based heat storage system. *J. Energy Storage* **2023**, *59*, 106506. [CrossRef]
94. Li, A.; Cao, F.; Zhang, W.; Shi, B.; Li, H. Effects of different thermal storage tank structures on temperature stratification and thermal efficiency during charging. *Sol. Energy* **2018**, *173*, 882–892. [CrossRef]
95. Lou, W.; Fan, Y.; Luo, L. Single-tank thermal energy storage systems for concentrated solar power: Flow distribution optimization for thermocline evolution management. *J. Energy Storage* **2020**, *32*, 101749. [CrossRef]
96. Khurana, H.; Majumdar, R.; Saha, S.K. Thermal stratification characteristics during simultaneous charging and discharging for different storage tank geometries with immersed discharging coil. *Appl. Therm. Eng.* **2023**, *225*, 120235. [CrossRef]
97. Khurana, H.; Tiwari, S.; Majumdar, R.; Saha, S.K. Comparative Evaluation of Circular Truncated-Cone and Paraboloid Shapes for Thermal Energy Storage Tank based on Thermal Stratification Performance. *J. Energy Storage* **2021**, *34*, 102191. [CrossRef]
98. Schwarzmayr, P.; Birkelbach, F.; Walter, H.; Hofmann, R. Standby efficiency and thermocline degradation of a packed bed thermal energy storage: An experimental study. *Appl. Energy* **2023**, *337*, 120917. [CrossRef]
99. Zanganeh, G.; Pedretti, A.; Zavattoni, S.; Barbato, M.; Steinfeld, A. Packed-bed thermal storage for concentrated solar power–Pilot-scale demonstration and industrial-scale design. *Sol. Energy* **2012**, *86*, 3084–3098. [CrossRef]
100. Le Roux, D.; Lalau, Y.; Rebouillat, B.; Neveu, P.; Olivès, R. Thermocline thermal energy storage optimisation combining exergy and life cycle assessment. *Energy Convers. Manag.* **2021**, *248*, 114787. [CrossRef]
101. Yang, Z.; Chen, H.; Wang, L.; Sheng, Y.; Wang, Y. Comparative study of the influences of different water tank shapes on thermal energy storage capacity and thermal stratification. *Renew. Energy* **2016**, *85*, 31–44. [CrossRef]
102. Kurşun, B.; Ökten, K. Effect of rectangular hot water tank position and aspect ratio on thermal stratification enhancement. *Renew. Energy* **2018**, *116*, 639–646. [CrossRef]
103. Marti, J.; Geissbühler, L.; Becattini, V.; Haselbacher, A.; Steinfeld, A. Constrained multi-objective optimization of thermocline packed-bed thermal-energy storage. *Appl. Energy* **2018**, *216*, 694–708. [CrossRef]
104. Nandi, B.R.; Bandyopadhyay, S.; Banerjee, R. Numerical modeling and analysis of dual medium thermocline thermal energy storage. *J. Energy Storage* **2018**, *16*, 218–230. [CrossRef]
105. Shaikh, W.; Wadegaonkar, A.; Kedare, S.B.; Bose, M. Numerical simulation of single media thermocline based storage system. *Sol. Energy* **2018**, *174*, 207–217. [CrossRef]
106. Bai, Y.; Yang, M.; Wang, Z.; Li, X.; Chen, L. Thermal stratification in a cylindrical tank due to heat losses while in standby mode. *Sol. Energy* **2019**, *185*, 222–234. [CrossRef]

107. Skuntz, M.E.; Elander, R.; Al Azawii, M.; Bueno, P.; Anderson, R. System efficiency of packed bed TES with radial flow vs. axial flow-Influence of aspect ratio. *J. Energy Storage* **2023**, *72*, 6. [CrossRef]

108. Esence, T.; Bruch, A.; Molina, S.; Stutz, B.; Fourmigué, J.-F. A review on experience feedback and numerical modeling of packed-bed thermal energy storage systems. *Sol. Energy* **2017**, *153*, 628–654. [CrossRef]

109. Lou, W.; Baudin, N.; Roux, S.; Fan, Y.; Luo, L. Impact of buoyant jet entrainment on the thermocline behavior in a single-medium thermal energy storage tank. *J. Energy Storage* **2023**, *71*, 108017. [CrossRef]

110. Wang, L.; Yang, Z.; Duan, Y. Influence of flow distribution on the thermal performance of dual-media thermocline energy storage systems. *Appl. Energy* **2015**, *142*, 283–292. [CrossRef]

111. Li, S.-H.; Zhang, Y.-X.; Li, Y.; Zhang, X.-S. Experimental study of inlet structure on the discharging performance of a solar water storage tank. *Energy Build.* **2014**, *70*, 490–496. [CrossRef]

112. Shafieian, A.; Bahrami, H.-R.; Roostaee, A.; Feyzi, S.S. Effects of different inlet configurations on the performance of solar storage tanks: A three-dimensional unsteady CFD simulation. *Case Stud. Therm. Eng.* **2023**, *45*, 103019. [CrossRef]

113. Vannerem, S.; Neveu, P.; Falcoz, Q. Experimental investigation of the impact of fluid distribution on thermocline storage performance. *J. Energy Storage* **2022**, *52*, 104864. [CrossRef]

114. Bellenot, G. *Study on the Influence of Fluid's Distribution over the Thermohydraulic Behaviour of a Single-Tank Dual-Media Thermal storageEtude de L'influence de la Distribution de Fluide sur le Comportement Thermohydraulique d'un Réservoir de Stockage Thermique Mono-Cuve Dual-Media*; Université Grenoble Alpes: Grenoble, French, 2020.

115. Soria-Verdugo, A.; Cano-Pleite, E.; Panahi, A.; Ghoniem, A.F. Partitioning of a wide bubbling fluidized bed with vertical internals to improve local mixing and bed material circulation. *Powder Technol.* **2022**, *408*, 117771. [CrossRef]

116. Morato-Godino, A.; Sánchez-Delgado, S.; García-Hernando, N.; Soria-Verdugo, A. Pyrolysis of *Cynara cardunculus* L. samples–Effect of operating conditions and bed stage on the evolution of the conversion. *Chem. Eng. J.* **2018**, *351*, 371–381. [CrossRef]

117. Hernández-Jiménez, F.; Soria-Verdugo, A.; Acosta-Iborra, A.; Santana, D. Exergy recovery from solar heated particles to supercritical CO_2. *Appl. Therm. Eng.* **2019**, *146*, 469–481. [CrossRef]

118. Cano-Pleite, E.; Hernández-Jiménez, F.; García-Gutiérrez, L.M.; Soria-Verdugo, A. Thermo-economic optimization of a novel confined thermal energy storage system based on granular material. *Appl. Therm. Eng.* **2023**, *224*, 120123. [CrossRef]

119. Soria-Verdugo, A.; Guil-Pedrosa, J.F.; Hernández-Jiménez, F.; García-Gutiérrez, L.M.; Cano-Pleite, E.; García-Hernando, N. Experimental analysis of a novel confined bed system for thermal energy storage. *J. Energy Storage* **2023**, *69*, 107972. [CrossRef]

120. McTigue, J.D.; White, A.J. A comparison of radial-flow and axial-flow packed beds for thermal energy storage. *Appl. Energy* **2018**, *227*, 533–541. [CrossRef]

121. Capocelli, M.; Caputo, G.; De Falco, M.; Mazzei, D.; Piemonte, V. Two-Channels Thermal Energy Storage Tank: Experiments and Short-Cut Modelling. *Zenodo* **2017**, 10008164. [CrossRef]

122. Capocelli, M.; Caputo, G.; De Falco, M.; Balog, I.; Piemonte, V. Numerical Modeling of a Novel Thermocline Thermal Storage for Concentrated Solar Power. *J. Sol. Energy Eng.* **2019**, *141*, 051001. [CrossRef]

123. Xia, L.; Zhang, P.; Wang, R.Z. Numerical heat transfer analysis of the packed bed latent heat storage system based on an effective packed bed model. *Energy* **2010**, *35*, 2022–2032. [CrossRef]

124. Zhu, Q.; Xuan, Y. Pore scale numerical simulation of heat transfer and flow in porous volumetric solar receivers. *Appl. Therm. Eng.* **2017**, *120*, 150–159. [CrossRef]

125. Guo, X.; Dai, R. Numerical simulation of flow and heat transfer in a random packed bed. *Particuology* **2010**, *8*, 293–299. [CrossRef]

126. Zhang, Z.; Yu, C.; Ci, Z.; Cao, L. A numerical study on the thermal storage properties of packer bed under different arrangements of PCM capsules. *Therm. Sci.* **2022**, *26*, 1345–1356. [CrossRef]

127. Lv, P.; Liu, L.; Lei, G.; Dong, H. Pore-scale numerical investigation on the thermal storage properties of packed-bed systems with phase change material microcapsules. *J. Clean. Prod.* **2023**, *405*, 137071. [CrossRef]

128. Flueckiger, S.M.; Garimella, S.V. Latent heat augmentation of thermocline energy storage for concentrating solar power—A system-level assessment. *Appl. Energy* **2014**, *116*, 278–287. [CrossRef]

129. Cheng, X.; Zhai, X. Thermal performance analysis and optimization of a cascaded packed bed cool thermal energy storage unit using multiple phase change materials. *Appl. Energy* **2018**, *215*, 566–576. [CrossRef]

130. Elfeky, K.E.; Ahmed, N.; Wang, Q. Numerical comparison between single PCM and multi-stage PCM based high temperature thermal energy storage for CSP tower plants. *Appl. Therm. Eng.* **2018**, *139*, 609–622. [CrossRef]

131. Elfeky, K.E.; Li, X.; Ahmed, N.; Lu, L.; Wang, Q. Optimization of thermal performance in thermocline tank thermal energy storage system with the multilayered PCM(s) for CSP tower plants. *Appl. Energy* **2019**, *243*, 175–190. [CrossRef]

132. Elfeky, K.E.; Mohammed, A.G.; Ahmed, N.; Wang, Q. Thermal performance of cascaded and combined sensible-latent heat storage tank under fluctuations in sunlight and electric demand. *Appl. Therm. Eng.* **2023**, *229*, 120575. [CrossRef]

133. Elsihy, E.S.; Mokhtar, O.; Xu, C.; Du, X.; Adel, M. Cyclic performance characterization of a high-temperature thermal energy storage system packed with rock/slag pebbles granules combined with encapsulated phase change materials. *Appl. Energy* **2023**, *331*, 120380. [CrossRef]

134. John, E.E.; Hale, W.M.; Selvam, R.P.; Brown, B.; Asme. Development and Performance Evaluation of High Temperature Concrete for Thermal Energy Storage for Solar Power Generation. In Proceedings of the ASME International Mechanical Engineering Congress and Exposition (IMECE), Denver, CO, USA, 11–17 November 2011; pp. 1207–1213.

135. Motte, F.; Bugler-Lamb, S.L.; Falcoz, Q. Thermocline Storage Filled with Structured Ceramics. Numerical Consistency of the Developed Numerical Model and First Observations. *High Temp. Mater. Process.* **2015**, *34*, 353–365. [CrossRef]
136. Strasser, M.N.; Selvam, R.P. A cost and performance comparison of packed bed and structured thermocline thermal energy storage systems. *Sol. Energy* **2014**, *108*, 390–402. [CrossRef]
137. Yu, C.; Qian, J.; Cao, D.; Chen, D.; Wu, L.; Zhang, C. Charging performance of structured packed-bed latent thermal energy storage unit with phase change material capsules. *J. Energy Storage* **2023**, *71*, 108157. [CrossRef]
138. Elsihy, E.S.; Liao, Z.; Xu, C.; Du, X. Dynamic characteristics of solid packed-bed thermocline tank using molten-salt as a heat transfer fluid. *Int. J. Heat Mass Transf.* **2021**, *165*, 120677. [CrossRef]
139. Xu, C.; Li, X.; Wang, Z.; He, Y.; Bai, F. Effects of solid particle properties on the thermal performance of a packed-bed molten-salt thermocline thermal storage system. *Appl. Therm. Eng.* **2013**, *57*, 69–80. [CrossRef]
140. Khurana, H.; Majumdar, R.; Saha, S.K. Experimental investigation of heat dispatch controllability through simultaneous charging-discharging and stand-alone discharging operations in vertical cylindrical sensible heat storage tank. *J. Energy Storage* **2022**, *54*, 105268. [CrossRef]
141. Yaïci, W.; Ghorab, M.; Entchev, E.; Hayden, S. Three-dimensional unsteady CFD simulations of a thermal storage tank performance for optimum design. *Appl. Therm. Eng.* **2013**, *60*, 152–163. [CrossRef]
142. Fernández-Seara, J.; Uhía, F.J.; Sieres, J. Experimental analysis of a domestic electric hot water storage tank. Part I: Static mode of operation. *Appl. Therm. Eng.* **2007**, *27*, 129–136. [CrossRef]
143. Dickinson, R.M.; Cruickshank, C.A.; Harrison, S.J. Charge and discharge strategies for a multi-tank thermal energy storage. *Appl. Energy* **2013**, *109*, 366–373. [CrossRef]
144. Szczęśniak, A.; Milewski, J.; Dybiński, O.; Futyma, K.; Skibiński, J.; Martsinchyk, A. Dynamic simulation of a four tank 200 m^3 seasonal thermal energy storage system oriented to air conditioning at a dietary supplements factory. *Energy* **2023**, *264*, 126106. [CrossRef]
145. Crandall, D.M.; Thacher, E.F. Segmented thermal storage. *Sol. Energy* **2004**, *77*, 435–440. [CrossRef]
146. McTigue, J.D.; White, A.J. Segmented packed beds for improved thermal energy storage performance. *IET Renew. Power Gener.* **2016**, *10*, 1498–1505. [CrossRef]
147. Biencinto, M.; Bayón, R.; Rojas, E.; González, L. Simulation and assessment of operation strategies for solar thermal power plants with a thermocline storage tank. *Sol. Energy* **2014**, *103*, 456–472. [CrossRef]
148. Palomba, V.; Frazzica, A. Application of numerical methods for the design of thermocline thermal energy storage: Literature review and critical analysis. *J. Energy Storage* **2022**, *46*, 103875. [CrossRef]
149. Szczęśniak, A.; Milewski, J.; Dybiński, O.; Futyma, K.; Skibiński, J.; Martsinchyk, A.; Szabłowski, Ł. Determination of Thermocline Heat Transfer Coefficient by Using CFD Simulation. *Energies* **2023**, *16*, 3150. [CrossRef]
150. Untrau, A.; Sochard, S.; Marias, F.; Reneaume, J.-M.; Le Roux, G.A.C.; Serra, S. A fast and accurate 1-dimensional model for dynamic simulation and optimization of a stratified thermal energy storage. *Appl. Energy* **2023**, *333*, 120614. [CrossRef]
151. Hoffmann, J.F.; Fasquelle, T.; Goetz, V.; Py, X. A thermocline thermal energy storage system with filler materials for concentrated solar power plants: Experimental data and numerical model sensitivity to different experimental tank scales. *Appl. Therm. Eng.* **2016**, *100*, 753–761. [CrossRef]
152. Cortés, E.; Gaviño, D.; Calderón-Vásquez, I.; García, J.; Estay, D.; Cardemil, J.M.; Barraza, R. Application of layer view factor method in high temperature thermal storage packed bed. *Appl. Therm. Eng.* **2024**, *236*, 121471. [CrossRef]
153. Ruiz, G.; Ripoll, N.; Fedorova, N.; Zbogar-Rasic, A.; Jovicic, V.; Delgado, A.; Toledo, M. Experimental and numerical analysis of the heat transfer in a packed bed exposed to the high thermal radiation flux. *Int. J. Heat Mass Transf.* **2019**, *136*, 383–392. [CrossRef]
154. Chen, L.; Wang, C.; Moscardini, M.; Kamlah, M.; Liu, S. A DEM-based heat transfer model for the evaluation of effective thermal conductivity of packed beds filled with stagnant fluid: Thermal contact theory and numerical simulation. *Int. J. Heat Mass Transf.* **2019**, *132*, 331–346. [CrossRef]
155. Sedighi, M.; Padilla, R.V.; Alamdari, P.; Lake, M.; Rose, A.; Izadgoshasb, I.; Taylor, R.A. A novel high-temperature (>700 °C), volumetric receiver with a packed bed of transparent and absorbing spheres. *Appl. Energy* **2020**, *264*, 114705. [CrossRef]
156. Johnson, E.; Tarı, İ.; Baker, D. A Monte Carlo method to solve for radiative effective thermal conductivity for particle beds of various solid fractions and emissivities. *J. Quant. Spectrosc. Radiat. Transf.* **2020**, *250*, 107014. [CrossRef]
157. Wu, H.; Zhao, H.; Hao, Z.; Liu, F.; Niu, F. A non-linear transform approach for conduction-radiation heat transfer in the extended thermal discrete element method. *Int. J. Heat Mass Transf.* **2021**, *176*, 121432. [CrossRef]
158. Khurana, H.; Majumdar, R.; Saha, S.K. Response Surface Methodology-based prediction model for working fluid temperature during stand-alone operation of vertical cylindrical thermal energy storage tank. *Renew. Energy* **2022**, *188*, 619–636. [CrossRef]
159. Trevisan, S.; Jemmal, Y.; Guedez, R.; Laumert, B. Packed bed thermal energy storage: A novel design methodology including quasi-dynamic boundary conditions and techno-economic optimization. *J. Energy Storage* **2021**, *36*, 102441. [CrossRef]